Thesis for the degree of Licentiate of Engineering

Reactions with relativistic radioactive beams and gamma multiplicities

“One, two, many” said the Crystal Ball

Simon Lindberg

CHALMERS
UNIVERSITY OF TECHNOLOGY

Department of Physics
Chalmers University of Technology
Göteborg, Sweden 2016

Reactions with relativistic radioactive beams and gamma multiplicities
“One, two, many” said the Crystal Ball
SIMON LINDBERG

Department of Physics
Chalmers University of Technology
SE-412 96 Göteborg
Sweden
Telephone +46 (0)31-772 10 00

Cover:
Energy deposited in Crystal Ball versus the number of crystals fired in that event. A selection on incoming ^{17}N is made and no target is used.

Chalmers Reproservice
Göteborg, Sweden 2016

Reactions with relativistic radioactive beams and gamma multiplicities
"One, two, many" said the Crystal Ball
SIMON LINDBERG
Department of Physics
Chalmers University of Technology

Abstract

Experiments with relativistic radioactive beams are used to study the properties of exotic nuclei. The experimental setup used in this thesis is a complex system of detectors for identifying and measuring the 4-momenta of all incoming nuclei and products created when the nuclei impinge on a reaction target. The high spatial resolution of the tracking detectors makes it impossible to align all the detectors with sufficient mechanical precision. Instead the measured tracks are used to calculate the exact detector positions during the data analysis. In this thesis a simplified and improved method is presented for the detector alignment.

In the target different types of reactions can take place. The reactions of most interest in this thesis are fragmentation and knockout reactions. In these reactions nucleons are removed from the nuclei, creating new isotopes which typically are in their excited state. If the excitation energy is lower than the particle emission threshold, the excitation energy is emitted as gamma radiation. The gamma multiplicity gives information about the excited states populated and the reaction mechanism. In this thesis radioactive beams ranging from proton-rich Li to neutron-rich F isotopes have been created and studied. The wide range of isotopes offers the possibility to compare the gamma multiplicities between different reaction channels and the different isotopes.

The analysis showed that the background contribution to the gamma multiplicity was too large to obtain any reliable results. Different approaches of reducing the background and possible explanations of the large contributions are discussed in the thesis.

Keywords: Radioactive Beams, R^{3}B, GSI, FAIR, Gamma Multiplicity, Calibration, Analysis, Virtual Alignment

Contents

Chapter 1

Introduction

Over 100 years have passed since Ernest Rutherford proposed the existence of an atomic nucleus. Since then much effort has been spent on trying to understand and explain the properties of nuclei. Many discoveries have been made on the way, leading to different theories and models of the atomic nucleus. Among the first models developed were the liquid drop model and the nuclear shell model [1, 2]. More recently developed models are the Nilsson model described in Ref. [3], or different *ab initio* methods, e.g. coupled-cluster methods [4], quantum Monte Carlo applications [5], perturbative expansions [6] or Green's function methods [7]. The reason for the existence of those different approaches is that all of them only are applicable in different parts of the chart of nuclides. This means that different methods have to be applied depending on which isotope is studied. The problems for all models of the nucleus are the nucleon-nucleon interaction, which is not fully understood, and the many-body character of the nucleus. A heavy nucleus consists of several hundred nucleons which all interact with each other. That is a very complicated system to solve and that is one of the main problems in finding a unifying model which can be applied on all known isotopes.

New developments on both, the theoretical and the experimental side, improve theories and knowledge about the nuclei. For theoretical research the constantly increasing computational power has been and still is an important driving force as well as refined theories concerning the nucleon-nucleon interactions and many-body models. On the experimental side, the facilities for experiments with radioactive beams developed in the last centuries play a key role. They have enabled studies of exotic nuclei situated in previously unreachable regions in the chart of nuclides. These nuclei are unstable and decay, hence they have to be produced during experiments. The possibility to study nuclei at the extremes, with an excess of neutrons or protons, has become an important tool in nuclear physics. The boundaries of possible experiments are also pushed with new facilities for experiments with radioactive beams. One of the world-leading facilities at the moment is RIKEN [8] in Japan, while the transition of GSI [9] to FAIR [10] in Germany will extend the possibilities further. It is not only the beam-producing facilities, which are improved but also the detectors of the setups used in the experiments with the beams. In this thesis the LAND-setup at GSI has been used. This setup will be greatly improved with, e.g. a new gamma detector [11,12] and a new neutron detector [13] for future experiments at FAIR.

The LAND-setup is used to perform kinematically complete measurements of reactions with relativistic radioactive beams. The 4-momenta of the incoming ion and all outgoing reaction products are measured and identified in terms of charge and mass. This allows studies of, e.g. resonances in unbound states, the electro-magnetic response of exotic nuclei, or the single-particle structure of exotic nuclei. A detailed description of the LAND-setup is presented in Ch. 2. To obtain the 4-momenta of the reaction products they need to be tracked through the setup. For this purpose, designated tracking detectors are used with high spatial resolution. These detectors cannot be mechanically aligned with sufficient precision for the tracking. Instead they are aligned as good as possible and moved virtually after the experiment, based on the measured tracks of the ions in the experiment. In Ch. 3 an improved method of this alignment is presented, which both simplifies the calibration and improves the result of the alignment.

The alignment of the detectors is important for the mass resolution of the reaction fragments. Obtaining the correct mass of the outgoing fragment is important for identifying, e.g. nucleon knockout or fragmentation reactions at the target. The experiment studied in this thesis uses radioactive beams of a wide range of nuclei. It includes beams of proton- to neutron-rich nuclei, ranging from Li to F, and provides an overview of an entire area of the chart of the nuclides. In Ch. 4 an attempt to use gamma multiplicities as probe for different final reaction channels is presented. The wide range of isotopes included in the beams makes it an unique opportunity to obtain an overview of the population and decay of excited states, not only for a large number of isotopes, but also for different reaction channels. The overview is useful to learn which isotopes are interesting for deeper analysis and which do not decay by gamma emission. Information on the reaction mechanism might also be obtained by comparing gamma multiplicities of different reaction channels, which populate the same isotope. In this setup it is not possible to detect isomers, though. That is because the measurements are made in-flight and before an isomer can decay, it has already left the experimental setup. During the analysis it turned out that the gamma multiplicity measurements suffered from very large background contributions, though. This made any investigation in the gamma multiplicity impossible. Different attempts of reducing the background and its origin are discussed in Ch. 4.

Chapter 2

Setup

The data analysed in this thesis was produced at the GSI Helmholtzzentrum für Schwerionenforschung in Darmstadt, Germany. The experiment took place during August and September in 2010 using the LAND-setup. A generic description of the setup can be found in Ref. [14]. The setup consists of a complex detector system designed to perform kinematically complete measurements of reactions with relativistic radioactive beams. If all 4-vectors of all reaction products are known, it is possible to reconstruct events kinematically. This allows studies of, e.g. resonance energies in unbound states and their structure, electromagnetic responses or the single-particle structure of exotic nuclei. To obtain the 4-vectors the mass, charge, track and velocity of the reaction products are measured. The experiments at GSI focus on exotic nuclei, i.e. nuclei with an excess number of neutrons or protons compared to the stable isotopes. This is of interest for the fundamental understanding of atomic nuclei and can be applied in e.g. astrophysics to understand the nuclear processes taking place within stars. The problem with exotic nuclei is that they decay and hence have to be produced when they are needed in order to not decay before measurements can be performed. Hence, to carry out the experiment it is not only the detector setup that is needed, but also a facility to create the nuclei of interest with the ability to transmit those nuclei to the experimental setup.

2.1 Beam production

The beam producing facility consists of a combination of accelerators for ions, ranging from single protons to uranium. In Fig. 2.1 the most important parts of the accelerator facility are shown. Ions are extracted from the ion source and are accelerated in the linear accelerator UNILAC creating a beam of stable ions. For experiments at lower energies, up to 11.4 AMeV, the produced beam can be sent to the experimental hall I, but to reach relativistic energies the beam is injected into the synchrotron accelerator, SIS18, which can accelerate uranium up to 1 AGeV[1]. From the synchrotron the beam can either be sent to the ESR (Experimental Storage Ring), or directly to the experimental hall II. To produce radioactive ions though, the FRS (FRagment Separator) [15] has to be used. At the entrance of the FRS the stable beam hits a target and by fragmentation reactions a wide range of different isotopes are created. After the target the beam consists of a mixture of both stable and radioactive isotopes.

In the FRS there are four independent stages, each with a 30° dipole magnet used to select the wanted isotope. Before and after the dipole magnets are quadrupole and sextupole magnets for focusing the beam. These stages are used to separate the different isotopes based on their magnetic rigidity. The magnetic rigidity defines how much a charged particle is deflected in a given magnetic field. It can be related to the mass, charge and velocity of the ion as $B\rho \propto \frac{A}{Z} \cdot \beta\gamma$, where $B\rho$ is the magnetic rigidity, A is the number of nucleons, Z is the nuclear charge of the ion, β is the velocity of the ion expressed in units of the speed of light c and $\gamma = \frac{1}{\sqrt{1-\beta^2}}$ is the Lorentz factor. In general the atomic charge of the ion should be used instead of the nuclear charge, but at relativistic energies most ions are fully stripped, i.e. they have no electrons which leads to the nuclear charge being equal to the ion charge. Since all the fragments have very similar velocities the selection can be made by adjusting the magnetic field to match the mass over

---

[1] With smaller mass to charge ratio the energy per nucleon can be increased, for protons energies up to 4.5 GeV can be reached.

charge ratio of the wanted isotope.

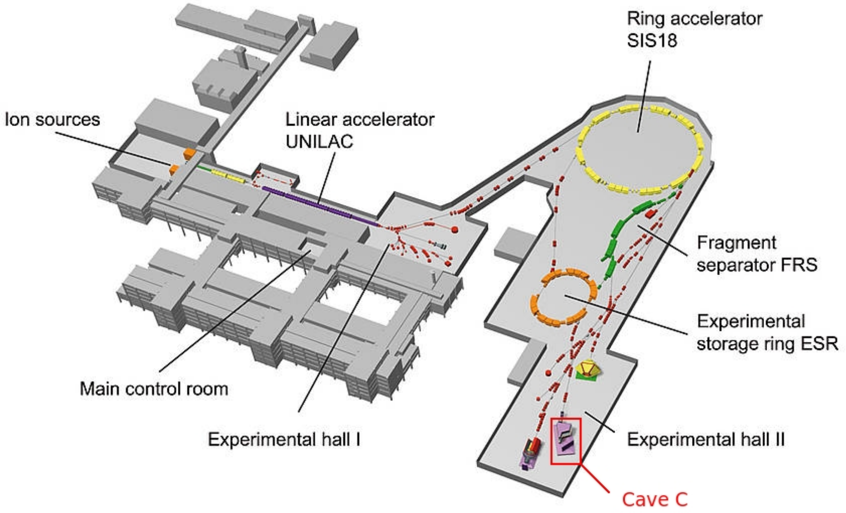

Figure 2.1: Overview of the beam production and experimental areas at GSI. The experiment was performed in Cave C which is marked in red in the figure. The figure is taken from Ref. [9].

To enhance the isotope selection further a degrader is used between the second and third dipole magnets. According to the Bethe-Bloch formula expressed in Eq. (2.1), where E is the energy of the ion, x is the distance travelled in the medium, m_e is the electron mass, c is the velocity of light, n is the number electron density, q is the ion charge, $\beta = \frac{v}{c}$ the velocity of the ion, e is the electron charge, ϵ_0 is the vacuum permittivity and I is the mean excitation potential of the target, the energy loss of the ions in the degrader is proportional to the square of their charge.

$$-\frac{\mathrm{d}E}{\mathrm{d}x} = \frac{4\pi}{m_e c^2}\frac{nq^2}{\beta^2}\left(\frac{e^2}{4\pi\epsilon_0}\right)^2\left(\ln\left(\frac{2m_e c^2\beta^2}{I(1-\beta^2)}\right) - \beta^2\right). \tag{2.1}$$

After the degrader the velocities of the different elements have changed differently, meaning that isotopes which had the same magnetic rigidity before the degrader now have been split apart. This let the final two dipole magnets improve the ion selection further. Finally the beam with the selected isotope can be directed either to the Experimental Storage Ring (ESR) or to the different caves in experimental hall II. For a more detailed explanation of the fragment separation, see Ref. [16].

The experiment analysed in this thesis is called S393 and was performed with a stable beam of ^{40}Ar at 490 AMeV. The production target used in the FRS was a 4 g/cm^2 Be target. The experimental setup was situated in Cave C which is marked in Fig. 2.1.

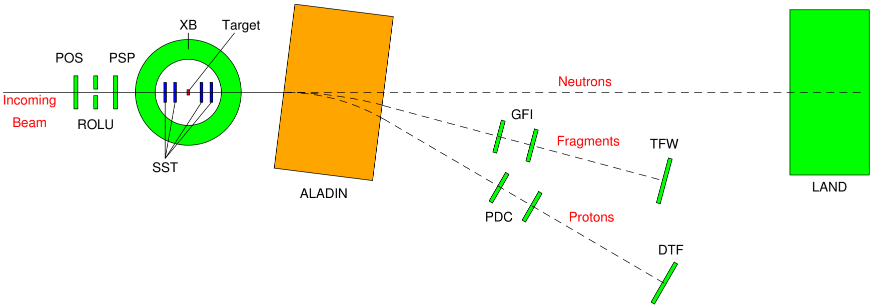

Figure 2.2: Schematic view of the LAND-setup. The beam enters from the left and the reaction target is in the centre of the Crystal Ball (XB). The large dipole magnet ALADIN deflects the reaction fragments into three different arms, one for neutrons, one for fragments and one for protons. The figure is not to scale.

2.2 Detector setup

The LAND-setup which was used for the experiment provides kinematically complete measurements of the reactions by measuring both time-of-flight, flight paths and energy losses of the incoming ion and all outgoing reaction products. A schematic view of the setup is shown in Fig. 2.2.

2.2.1 Incoming ions

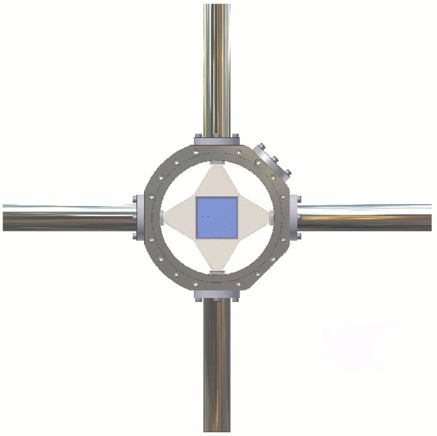

Figure 2.3: The POS detector used for time-of-flight measurements, both of incoming ions and outgoing reaction products. The blue square in the centre indicates the plastic scintillator and the light guides connect it to the four PMTs. Figure is taken from Ref. [17].

In Fig. 2.2 the incoming radioactive beam enters from the left hitting a plastic scintillator called POS. Despite its name which was given for historical reasons, it is only used as start and stop detector for time-of-flight measurements and not for position measurements. The stop signal is used for the time-of-flight measurement from the FRS where the detector giving the start signal, called Sci2, is situated. The start signal from POS is used to measure the time-of-flight in the setup and the stop signals are given by the time-of-flight walls at the end of the setup. The POS detector covers an area of 5.5×5.5 cm^2 and has four light guides to four PMTs[2]. A schematic view of the detector can be seen in Fig. 2.3.The ROLU detector is situated behind the POS detector. It is an active veto and is used to suppress beam halos and ensures that the incoming ions that are recorded hit the target. It consists of four plastic scintillators placed to form an aperture in between them, which can be seen in Fig. 2.4. If an ion hits any of the scintillators it is considered to be

---

[2] Photo Multiplier Tube, converts and amplifies light into an electrical signal using the photoelectric effect and photo-electron multiplication.

too far from the desired beam position and the signal can be used to discriminate that event. The size of the open square can be adjusted by moving the scintillators allowing for broader or narrower beam profiles.

When the ions have passed the ROLU they hit the PSP detector, which measures both the energy loss in the detector and the position of the hit. It is a silicon detector, which has an active area of 4.5×4.5 cm^2 and is 300 μm thick. The front side forms a p-n junction by implanted boron ions and serves as an anode while the back side works as a cathode. On the anode side there are four signal readouts, one in each corner of the detector. The relative differences of the signal amplitudes between the readouts are used to extract the hit position in the detector. On the cathode side there is a single readout giving the total energy deposited in the detector. Since the energy loss is proportional to the square of the atomic charge of the ion, this information gives the number of protons in a fully stripped ion. Together with the time-of-flight measurement and the known magnetic rigidity setting of the FRS, this is sufficient to fully identify the incoming ion, which impinges on the target.

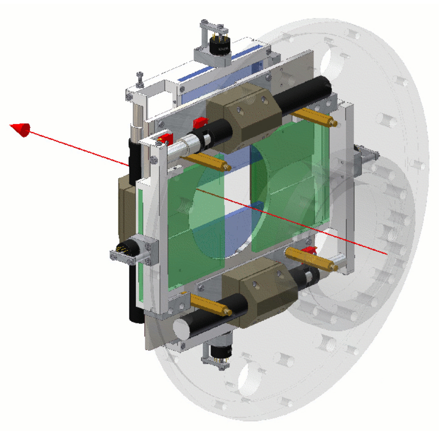

Figure 2.4: The ROLU is built up by four independent plastic scintillators, in blue and green in the figure. It is used to discriminate ions too far from the centre of the beam. The opening between the scintillators can be adjusted for tuning the allowed width of the beam. The figure is taken from Ref. [17].

2.2.2 Detectors around the target

Before the ions reach the target they pass through two double sided silicon strip detectors called SSTs. They perform position measurements and have a resolution of 50 μm, combined they give the direction of the incoming ions towards the target. They also provide the energy loss in the detector, which can be used for particle identification. The SSTs cover 7.2×4.0 cm^2 and are 300 μm thick. The vertical strips have a pitch size of 27.5 μm, but only every fourth channel is read out while the others are left floating. The horizontal strips have a pitch size of 104 μm and all of them are read out. A picture of one SST detector is shown in Fig. 2.5. Behind the target are two more SSTs which, like the ones in front of the target, are used for tracking and energy loss measurements. In this case it is the reaction fragments that are tracked, though.

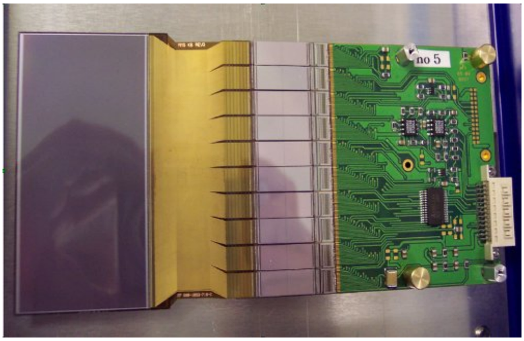

Figure 2.5: A photo of one SST detector. The grey part to the left is the 40×72 mm^2 active area of the detector. The figure is taken from Ref. [17].

Surrounding the target, and the four SSTs, is a 4π-gamma detector called Crystal Ball (XB). It consists of 162[3] NaI(Tl) crystals, each readout by a PMT, forming a 20 cm thick spherical shell around the target area [18]. The crystals come in four different shapes but all cover the same solid angle as seen from the target. Originally it was constructed for detecting gammas, but has been upgraded to detect also protons and neutrons scattered at large angles at energies of a

---

[3] In reality only 159 are present because three crystals are removed to allow the incoming and outgoing beam to pass and one for the holding structure of the target chamber.

few hundred MeV. To measure the energy deposited both by gammas and protons there are two independent readouts, the low-energy readout is taken from the anode, while the high-energy readout is taken from the last dynode of the PMTs. This dual readout is only used in the 64 most forward oriented crystals in the beam direction. Because of the strong kinematic forward focus in the reactions, most reaction products are scattered at very small angles and do not interact with the Crystal Ball but enter ALADIN, a wide aperture dipole magnet. The few products which are scattered at larger angles still have a large momentum in the forward direction and hence hit the most forward oriented crystals in the Crystal Ball.

One effect which have to be taken into account in the energy measurements of the gammas in the Crystal Ball is the Doppler effect. The gammas originate from excited states in the ions which are travelling at velocities at more than half the speed of light. This leads to shifts in the energy spectrum of the gammas depending on the relative direction of the gamma and the ion according to Eq. (2.2), which is the relativistic Doppler effect for a source emitting a gamma with energy E_s travelling away from an observer at velocity v at an angle θ from the detector measuring the energy E_o.

$$E_o = \frac{E_s}{\gamma(1 + \frac{v}{c}\cos\theta)}. \tag{2.2}$$

If the angle is known it is possible to correct for the Doppler effect. The direction of the ion is given by the SSTs as explained earlier, but the direction of the gamma is only measured by which crystal is hit in the Crystal Ball. With higher granularity the angle would be more precise and the corrected energy would be better reconstructed. Still, if the exact angle is not known, the energy resolution decreases with the uncertainty in the angle, this is known as Doppler broadening. The Crystal Ball has, as mentioned earlier, 162 crystals, even if this is enough to do the Doppler correction the Doppler broadening is still a problem. That is one reason why a new detector called CALIFA [11,12] with a much higher granularity is constructed for future experiments.

2.2.3 ALADIN

Even though ALADIN is not a detector, it is a central part of the setup. It is used to deflect the reaction products, deflecting them into three different arms based on their magnetic rigidity. Neutrons are naturally unaffected by the magnetic field, protons are deflected the most (about 30 degrees) with $\frac{A}{Z} = 1$ and the heavier fragments with $\frac{A}{Z} \sim 2 - 3$ end up in between (around 15 degrees). The magnetic field in ALADIN can be adjusted to obtain the right deflection angle depending on the energy and magnetic rigidity of the incoming radioactive beam. There is no direct measurement of the magnetic field, but it is set by the current in the magnet, which can be adjusted between 0 and 2500 A. Even though the magnetic field is not measured, it is still needed to track the reaction products which is described in Ch. 3. To solve this, the magnet current has to be related to the magnetic field. Another problem is that the magnetic field is not homogeneous in the entire magnet, meaning that a current cannot be associated with one specific magnetic field. The field does also not scale linearly with the current. Instead field maps have to be measured for different currents. This was done by setting the magnet current to a fixed value and then measure the magnetic field in different positions in the magnet[4], creating a 3-dimensional map of the magnetic field. This procedure is repeated for different magnet currents, so each current has its own field map. For ALADIN, field maps have been measured for 0 A, 500 A, 1100 A and then every 200 A up to 2500 A.

Ideally there would exist a field map for each current that is used in the magnet, but this is not practically possible. Instead interpolations are done between the field maps, which have been measured, to calculate the magnetic field for a given current. This is not as accurate as the measured field maps, but there are also other problems with the field maps. The main problem is the hysteresis of the magnet, meaning that the magnetic field is not the same for the same current depending on how the current is reached[5]. As a consequence it is not even sure

---

[4] And also outside to include the stray field in the field map.

[5] If it is decreased from a higher value or increased from a lower.

that the measured field maps are correct even if the current is the same as during the field map measurement. It is not possible to do anything about this, but it is useful to know about it during the tracking.

2.2.4 Behind ALADIN

Since the different reaction products are separated by ALADIN, also the detector setup is divided downstream of it. There are three different arms, one for neutrons, one for heavy fragments and one for protons. In the neutron arm there is only one detector, LAND (Large Area Neutron Detector). It covers an active area of 2×2 m^2 and is 1 m thick [19]. It is built up of ten planes where each plane consists of 20 bars with alternating plastic scintillating material and iron as seen in Fig. 2.6. The reason for using the iron is that it has a larger cross section for reactions with neutrons than plastic, hence it increases the efficiency of the detector. The main tasks of LAND is to determine the neutron multiplicity and the time-of-flight from the POS detector for each event. The multiplicity is used to determine the reaction at the target and the time-of-flight for extracting the momenta of the neutrons.

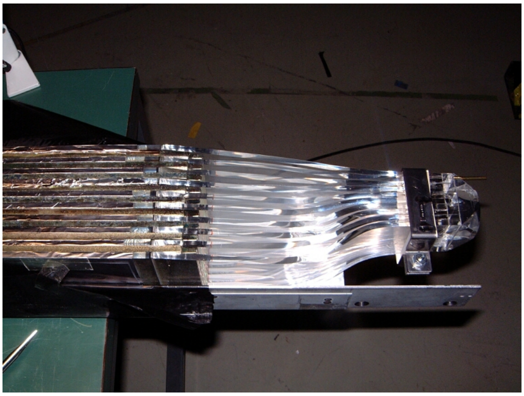

Figure 2.6: A photo of a part of one of the 200 LAND bars. It consists of alternating 0.5 cm thick plastic and iron building up a 10 cm thick bar. In both ends are light guides to a PMT. The photo is taken from Ref. [17].

The fragment arm consists of two fibre detectors named GFI. They are used to track the fragments behind ALADIN. Each detector has an active area of 50×50 cm^2 consisting of 1 mm thick scintillating fibres [20]. One end of each fibre is coupled to a position-sensitive PMT which indicates which fibre has fired. Since the fibres are oriented vertically this gives a good position resolution in the x-direction, which is similar to the thickness of the fibres, 1 mm. The other ends of the fibres are connected to a regular PMT which is used to provide a timing signal from the detector. With the hit positions in both GFIs the track of the ion behind ALADIN can be determined.

The last detector in the fragment arm is the TFW, its main purpose is to measure the time-of-flight from the POS detector and the energy loss. Combining this information with the track given by the GFIs and SSTs, the outgoing fragment can be identified in terms of its nuclear charge and mass on an event by event basis and the 4-momentum is accessible. The TFW is a detector consisting of 32 plastic scintillating paddles in two layers, 18 vertical paddles and 14 horizontal paddles.

The protons are handled in a similar way as the fragments. First they impinge on the tracking detectors, in this case two drift chambers. They both consist of 144 vertical wires and 112 horizontal wires providing position resolutions around 200 μm in both x and y-direction. At the end of the proton arm is a plastic scintillation detector for measuring the time-of-flight from the POS detector. Combining the track information with the time-of-flight provides the momentum of the outgoing protons.

Combining all detectors in the setup it is possible to uniquely identify all incoming ions in terms of mass, charge and momentum. The setup also detects and measures all reaction products. That includes gamma photons, neutrons, protons and heavier fragments. With the complete information of what went in and what came out, the reaction itself can be reconstructed and analysed in detail.

2.3 Triggers

The probability of having a nuclear reaction in this type of experiments is usually around a few percent, depending on target thickness. To collect enough statistics to do any meaningful analysis it is important to collect as much and as relevant data as possible during an experiment. The data recorded by the detectors have to be collected and stored for later analysis by the DAQ (data acquisition system). During this time the detectors do not record any new data, this is known as dead time of the system. To increase the efficiency of experiments it is good to be able to decide if an event is an interesting event or not before it is collected by the DAQ. For this purpose each detector creates a logic signal, that is sent to a trigger logic module, which can be used to decide if an event should be stored or if it should be ignored.

2.3.1 Logic detector signals

The logic signals indicate if a detector has been hit or not. These signals are created from analogue signals with amplitudes proportional to the energy deposited in the detectors. If the amplitude is above a set threshold value the logical trigger signal is set to one, otherwise it is set to zero. Apart from the logic detector signals there are also two internal signals in the trigger module. Those are the onspill signal and the early-pile up signal. The onspill signal indicates if the beam is on or off. During an experiment the beam is not transmitted to the setup all the time, but it comes in intervals determined by the synchrotron. Typically the beam is transmitted to the setup from a second at the time up to maximum 10 seconds; this is what is called onspill. Offspill is the time in between the beam intervals when no beam is transmitted to the setup, this time is usually about the same length or shorter than the onspill interval.

The early-pile up signal indicates if two ions have been detected too close to each other in time in POS. For this experiment the condition was that ions had to be separated at least by 5 μs. This is to avoid events where signals originating from different ions are added in a detector, which leads to a signal from the detector that cannot be used because the contribution of the two ions cannot be disentangled. Different detectors have different conditions for their logic signals to be active. The signals which are of interest for this thesis and their condi-

Table 2.1: The different logic signals used in the analysis performed in this thesis and their conditions.

Pos !ROLU	At least two channels in POS above threshold and none in ROLU.
TFW	At least two channels in the TFW above threshold.
XB or	At least one channel above threshold in the Crystal Ball.
XB or delayed	Same as XB or but time delayed.
XB sum	At least one high energy deposit in the Crystal Ball.
XB sum delayed	Same as XB sum but time delayed.
XB L&R	At least one high energy deposit in both the right and left half of the Crystal Ball.

tions, are listed in Tab. 2.1. The trigger handling module can require coincidences between different logic detector signals and that is why some signals are duplicated with a time delay. By combining different signals, a decision can be made if this event is worth saving for analysis or not. Which signals have been involved in the trigger decision for a given event is also stored in what is called the trigger pattern (Tpat).

2.3.2 Trigger patterns

The trigger patterns are used in the analysis to select events involving certain detectors. For each event several trigger patterns can be present[6]. To save the information about which trigger patterns have been used in the event each pattern is given a number, in this experiment ranging from 1 to 15. They are arranged such that the first 8 patterns are used for onspill events and the last 7 are used for offspill events. Then a binary system is used where the first trigger pattern is related to the first bit, the second pattern to the second bit and so on up to bit 15 which is related to the 15$^{\text{th}}$ trigger pattern. If the condition for a trigger pattern has been fulfilled in an event the bit related to that pattern is set to 1 and otherwise it is 0. This is a simple way of saving all the information about the triggers in an event in one single

---

[6] There will only be one readout of the event, even if several Tpats are active.

Table 2.2: The different trigger patterns used in this thesis, their corresponding numbers and their conditions. A “!” indicates a logic NOT-condition and “&” indicates an AND-condition. Number 1-8 are triggers for onspill events, while 9-15 indicate offspill events.

1	**Minimum bias**	onspill & POS !ROLU
2	**Fragment**	onspill & !early pile up & POS !ROLU & TFW
4	**XB sum**	onspill & !early pile up & POS !ROLU & XB sum
9	**XB muon**	!onspill & !(POS !ROLU) & XB sum delayed
12	**XB gamma**	!onspill & !(POS !ROLU) & XB or delayed
15	**XB L&R-muon**	!onspill & !(POS !ROLU) & XB L&R

number. The trigger patterns which have been used in this thesis are listed in Tab. 2.2.

The difficulty of fulfilling the different trigger patterns differs between the different patterns. For example it is obvious that the minimum bias condition is easier to fulfil than the XB sum condition simply because both have the same conditions but the latter has an additional two conditions to fulfil. The consequence of this is that there are many more triggers with the Minimum bias pattern than the XB sum pattern. To even this out and prevent that only events with a certain trigger pattern are recorded downscale factors are applied to each trigger pattern. This factor tells how often an event should be recorded for a certain trigger pattern. Trigger patterns with many conditions to fulfil usually are used with a lower downscale factor than a trigger pattern with less conditions to fulfil.

2.4 The LAND02 package

When performing experiments the data is stored in so called list mode dump files (lmd-files). Everything stored in these files are raw data from each readout channel. To get any physics out of the data it first has to be calibrated and combined according to the physical detectors. For this purpose the LAND02 package has been developed. It is used to reconstruct the data, i.e. convert the raw data into energies, positions and times, and unpack the data into so called root-files. These files can be opened with the program *root*, which is developed for analysis of high energy nuclear physics experiments. It is used both in the process of extracting the calibration parameters of the detectors and in the physics analysis. More information about the program can be found in Ref. [21]. The calibration of the data is done in several steps and with LAND02 it is possible to choose at what level the data written to the root-files should be, i.e. how much should be reconstructed.

The data can be unpacked at six different levels. These are RAW, TCAL, SYNC, DHIT, HIT and TRACK levels. There are some differences between the different detectors in the setup concerning the calibration at each level, but in general the structure is as follows: At RAW level all data is unpacked as it was stored in the lmd-files, i.e. completely uncalibrated. In the TCAL level the time and energy calibration has begun. The time signals have a gain and offset relating the raw data to a times in ns. For the energy signals an offset has been applied to subtract background contributions from the electronics. At SYNC level offsets to all time signals have been applied to ensure that all channels have a common 0. The energy signals now have gains and offsets to relate the raw data to energies in MeV.

At DHIT level the hit positions in the detectors are calculated and expressed in detector specific coordinate systems. The energy and time is also expressed for the detector instead of each individual channel of the detector. The HIT level is not that different from the DHIT level but all positions have been transformed to a general coordinate system where the origin usually is in the centre of the detector, positive x is pointing left and y up when looking in the direction of the beam. The final level, TRACK is a bit different from the other levels. It combines information from different detectors to track the ions. This is used to extract information about the mass, charge and momenta of the incoming ions. For more information about the LAND02 package see Refs. [17, 22].

Chapter 3

The TRACKER

The TRACKER is a program developed by R. Plag for the LAND-setup to identify the mass of the outgoing fragment after the reaction at the target. The reason the TRACKER is only needed for outgoing and not for incoming ions is the difference between the magnets in the FRS and ALADIN. In the FRS long magnets[1] with a limited aperture are used. ALADIN on the other hand has a large acceptance while being rather short, about 1.5 m. Another difference is that the magnetic field in the FRS dipole magnets are measured directly and the magnets are ramped up and down repeatedly when the field is changed to avoid the influence of the hysteresis of the magnets. In ALADIN only the magnet current is measured. Because of the small aperture in combination with the long magnets, a much more precise magnetic rigidity can be chosen in the FRS than in ALADIN. The magnetic rigidity selected in the FRS, makes it possible to obtain the mass of the ion from the time-of-flight. This is true at least for lighter fragments as used in this experiment; for heavier fragments corrections for the path of the fragments have to be applied before the mass can be obtained.

The TRACKER works iteratively, comparing measured data with calculated tracks on an event-by-event basis. The calculations are done by taking start parameters, i.e. charge, mass and velocity from the mea-

---

[1] The dipole stages are around 36 m.

sured data and then using the Runge-Kutta [23] method to calculate the path of the ion through ALADIN. By applying small variations on the start parameters[2] the resulting track also changes. When the calculated and measured data agree, the right mass and velocity have been found and hence also the mass of the fragment. However, before this procedure works it is necessary to calibrate the tracker. That means the positions of all detectors should be defined. This is a challenging task since several of the detectors have spatial resolutions well below a millimetre while they are separated by several meters. Hence it is almost impossible to measure the positions of the detectors with sufficient precision in any conventional way. In this section an alternative method is presented, which instead uses the measured tracks to calculate the detector positions.

3.1 Working principle of the tracker

The tracker can be operated in three main modes: forward, backward and mixed mode [24]. The difference between these modes lies in the selection of the detectors that define the track to start the iteration from. In forward mode, the initial track is defined by the detectors in front of ALADIN, usually the two SSTs behind the target. In backward mode, the track is defined by the detectors behind ALADIN, usually the two GFIs. In mixed mode, the result from forward and backward tracking is joint together to find the optimal track. In this work the forward tracking mode has been used unless stated otherwise.

For the tracker to work it needs some basic information about the fragment to track and about the setup. This information is provided in two different files, one text-based configuration file, which the tracker reads at start up and one C++ file which is used in the compilation of the program. The minimum information needed is the positions and resolutions of the detectors involved in the tracking, i.e. the two SSTs behind the target, the two GFIs, and the TFW. More detectors can be used but are not necessary. Furthermore the magnitude of the

---

[2] Only the mass and velocity, the charge is fixed.

magnetic field of ALADIN is needed. The tracker uses this to select the field maps it applies. The magnetic field of ALADIN has been measured at different currents applied to the magnet as mentioned in Sec. 2.2.3. For each position in ALADIN the tracker calculates the magnetic field by interpolating between the two field maps closest to the set ALADIN current. Since the Lorentz force is proportional to the atomic charge of the ion, this information is also necessary. It is obtained from the energy loss in the SSTs and/or the TFW, and entered into the C++ file. Since the energy loss in material is proportional to the square of the atomic charge, the different charges can be easily identified as shown in Fig. 3.1 where the energy deposited in the TFW is plotted for incoming ^{18}C.

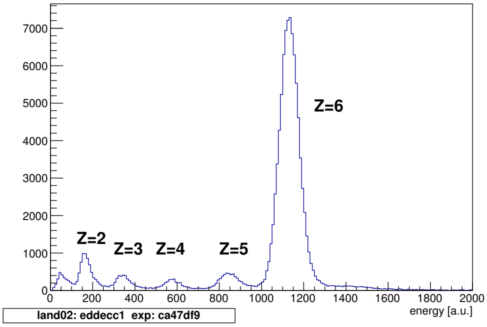

Figure 3.1: The energy loss in the TFW with ^{18}C impinging on the target. The large peak is the unreacted beam with charge $Z = 6$. The smaller peaks results from reacted ions, which have lost protons in reactions[3].

When all information is present the tracking can start. The first thing the tracker does is to calculate a start approximation. Since the charge is given in the configuration file the TRACKER only needs to calculate the mass, velocity and direction of the fragment. The velocity is taken from the time-of-flight measurement between the FRS and POS detectors and corrected for the energy loss in the detectors between POS and target. As a start approximation it is assumed that the ion did not react in the target,

---

[3] The information in the lower left box is internal information for reproducing the data analysis.

i.e. incoming and outgoing ions are identical and so the mass can be taken from the incoming particle identification [25]. The direction is defined by the positions in the SSTs[4] and this direction is fixed for all iterations. The tracker calculates the hit position in the centre of the target and the entering position into ALADIN by extrapolating from the SSTs. The velocity of the ions are corrected for the energy loss in the detectors on their way to ALADIN. In ALADIN the tracking is done with a Runge-Kutta method in very small steps [26], typically only a few millimetres depending on the magnetic field. In each step the magnetic field is updated according to the measured field map. This method gives an accurate tracking of the fragment through the entire magnetic field and in the end a precise direction of the fragment out of the magnet. With the direction of the fragment behind ALADIN, the hit positions in the GFIs and TFW can be calculated. These positions can be compared with the measured positions to see how well the tracking agree with the data. It also takes into account the time-of-flight from the target to the TFW when comparing. Depending on how well the tracked and measured data agrees in the GFIs and TFW, the tracker calculates new start values. With the new start values the tracking starts all over again. In this way it continues until the differences between the tracked and measured data are within the resolution of the detectors. When this has been achieved, the mass and velocity of the fragment is stored together with information about the tracking in a root tree.

3.2 Calibrating the TRACKER

Before the tracker can be used, it has to be calibrated. To get the measured and calculated hit positions to agree the detector positions in the calculations have to be identical to those in the physical setup. A first approximation can be achieved by measurements in the setup, but the precision is not good enough to allow precise tracking. The fine tuning of the detector positions has to be done with help of the measured data.

---

[4] In forward tracking mode.

The calibration of the tracker is done in several steps. The first thing to do is to align the SSTs. This is done with a program called Millepede II [27]. This is a program developed for aligning detectors. It makes use of the measured tracks in the data and optimises the detector positions to fit all measured tracks. This might sound simple but is not when the number of tracks to fit are several millions. When the SSTs are aligned the next step is aligning the detectors behind ALADIN, the GFIs and TFW. For this calibration the tracker itself can be used.

Since the TRACKER is not a newly developed program it has of course been calibrated before. This has been a tedious task though, and the calibrations have not been consistent between different users and runs in the experiments. To simplify the calibration of the TRACKER the author has developed a new calibration method, which also improved the result of the calibration. The new method uses three scripts, including one script providing Millepede II with useful data, one script for calibrating the incoming time-of-flight and one script for calibrating the detectors behind ALADIN with the help of the tracker.

3.2.1 Millepede II

Millepede II [27] consists of two main programs, Mille and Pede. The Mille part comes in two different versions, one written in Fortran 90 and one in C++. In this work, the C++ version has been used. Its task is to create a binary file with information on all the tracks to use for the optimisation of the detector positions. This binary file is in the next step used by Pede to calculate the optimal detector positions. In Fig. 3.2 a possible scenario is illustrated where the top figure shows two tracks hitting the SSTs which are not perfectly aligned. In the bottom figure least square fits have been applied to the hit positions from the two tracks under the assumption that the detectors are aligned. The basic principle of Millepede is that it tries to minimise the total error between the calculated tracks and the data for all events simultaneously by virtually adjusting the detector positions. In this case each detector can be adjusted in three different ways. They can be moved in x and y-direction, i.e. perpendicular to the beam, and they can be rotated

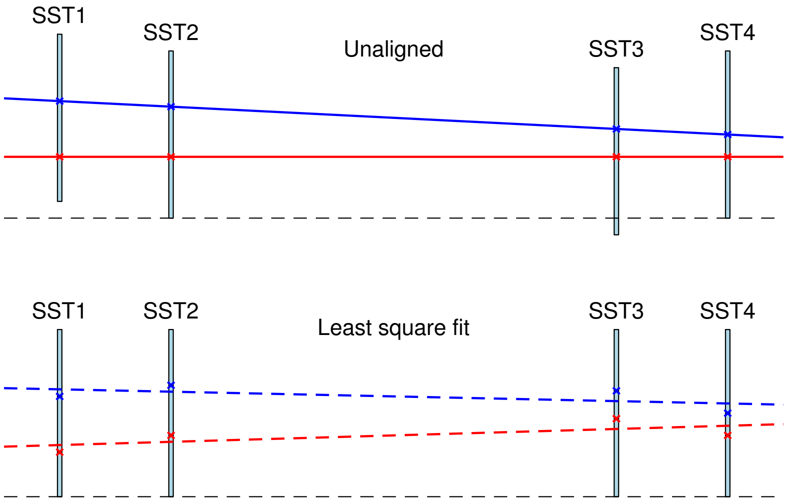

Figure 3.2: Top illustration shows a possible misalignment between the SSTs and two example tracks of ions. The bottom illustration shows how the least square fit would be affected with the assumption that the detectors were aligned.

around the beam axis. Since the movements of the detectors are just virtual, the measured data have to be modified corresponding to the movements of the detectors. These corrections are done in the following way:

$$x_c = (x_m - \delta x) \cdot \cos\,\omega + (y_m - \delta y) \cdot \sin\,\omega \tag{3.1a}$$

$$y_c = (y_m - \delta y) \cdot \cos\,\omega - (x_m - \delta x) \cdot \sin\,\omega, \tag{3.1b}$$

where x_c and y_c are the corrected hit positions, x_m and y_m the measured hit positions, δx and δy are the movements of the detectors in each direction and ω is the rotation angle around the beam axis.

Millepede distinguishes parameters into global and local parameters. Global parameters do not change between events, while local parameters do. In this case this means that detector positions are global parameters, while parameters defining the track of an ion are local. The data that has to be included in the binary file Mille creates, is the number of global and local parameters, the residual at each detector, the derivatives for all global and local parameters, an error estimate of each measurement, and a label for later identification of the global parameters. The derivatives describe how the hit position in a detector changes, given a small variation of the variable. The residual is the difference between the measured positions and the calculated position from the least square fit.

The least square fit is done with the assumption that all the detectors are aligned, even though this assumption may be wrong[5]. In Fig. 3.2 an example of the result of this assumption is illustrated. From the fit, four local parameters are extracted, two offsets and two angles, one for each direction, x and y. Each detector has one residual in each direction, which are[6]

$$x_r = x_c - (x_0 + dxdz \cdot z) \tag{3.2a}$$

$$y_r = y_c - (y_0 + dydz \cdot z), \tag{3.2b}$$

where x_c and y_c are the positions calculated in (3.1), x_0, y_0, $dxdz$ and $dydz$ are the parameters extracted from the least square fit and are the offsets and the angles of the tracks, while z is the position of the detector along the beam line direction.

For each parameter, both global and local, the derivatives of the residuals also have to be calculated. This is for Millepede to know how the residuals are affected by changing that specific parameter. By combining (3.1a) with (3.2a), and taking the derivatives, the following

---

[5] If it was right no calibration would be needed.

[6] The script calculating the residuals actually corrects the detector movements of the calculated positions and not of the measured, but this only affects the sign of the residuals and derivatives, and the alignment result is still the same.

results are obtained

$$\begin{aligned}\frac{\mathrm{d}x_r}{\mathrm{d}\delta x} &= -\cos\ \omega\\ \frac{\mathrm{d}x_r}{\mathrm{d}\delta y} &= -\sin\ \omega\\ \frac{\mathrm{d}x_r}{\mathrm{d}\omega} &= -(x_m-\delta x)\sin\ \omega + (y_m-\delta y)\cos\ \omega\\ \frac{\mathrm{d}x_r}{\mathrm{d}x_0} &= -1\\ \frac{\mathrm{d}x_r}{\mathrm{d}dxdz} &= -z.\end{aligned}$$

As mentioned earlier the detectors are assumed to be aligned, this means that $\delta x = \delta y = \omega = 0$ and the derivatives simplify to

$$\begin{aligned}\frac{\mathrm{d}x_r}{\mathrm{d}\delta x} &= -1\\ \frac{\mathrm{d}x_r}{\mathrm{d}\delta y} &= 0\\ \frac{\mathrm{d}x_r}{\mathrm{d}\omega} &= y_m\\ \frac{\mathrm{d}x_r}{\mathrm{d}x_0} &= -1\\ \frac{\mathrm{d}x_r}{\mathrm{d}dxdz} &= -z.\end{aligned}$$

This is also done for the y variables by combining (3.1b) with (3.2b) and calculating the derivatives.

When Mille has created the binary file, Pede can use it to calculate the optimal detector setup. This optimisation can be performed with a number of different methods. Which method to use depends mainly on the number of parameters to optimise. The standard method is matrix inversion and this method is used for this work. The solution method is defined in a configuration file which is read by Pede. In this file, conditions on the different global variables can also be set. They can be fixed so that Pede cannot change their positions or they can

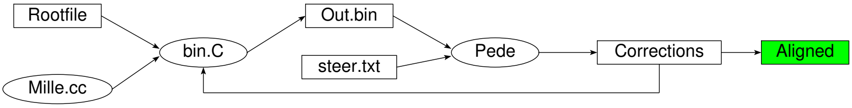

Figure 3.3: A flow chart of the SST alignment using Millepede. The data is taken from a root file and Mille.cc is used to create a binary file with all relevant data. The selection of events and calculations of residuals and derivatives are done in bin.C. Pede calculates the position corrections from the binary file and a configuration file called *steer.txt*. If the errors are smaller than the corrections the procedure starts over, but if the errors are larger the system is considered to be aligned.

be coupled to each other to fulfil certain conditions limiting how their position and orientation can be adjusted. In this case two detectors have to be fixed in their x and y positions and one in its rotation angle. This is necessary because if all detectors were allowed to be moved around freely there would exist an infinite amount of solutions to the alignment problem. For each solution the detectors could all be moved the same distance to create a new solution. By fixing two detectors in space this is no longer possible.

The output of Pede provides both the corrections of the global parameters and error estimates of the corrections. The errors tell how well aligned the detectors are. If the errors are large compared to the position corrections the alignment is good, but if the corrections are much larger than the errors, Millepede has added large corrections to the detector position. If this happens, it is a good idea to run Millepede again with the new detector positions. The calibrations script checks if the corrections are smaller than the errors; if that is not the case a new calibration is done. The general working principle of the SST alignment script is shown in Fig. 3.3.

3.2.2 Incoming time-of-flight

With the SSTs aligned, the next step is to calibrate the detector positions behind ALADIN. In this case not Millepede but the tracker itself is used. It is, however, important that the incoming time-of-flight has been calibrated first. Since the velocity of the fragment is calculated from the time-of-flight between the FRS and the POS detector, and this velocity is used for calibrating the tracker, it is important that the incoming time-of-flight is correct. As mentioned in Sec. 2.4 the conversion from the raw data to time signals is based on a linear function, one value for the offset and one value for the gain. Due to small changes in the environment of the setup during the experiment, such as temperature fluctuations, the performance of the detectors can change over time, and hence the calibration parameters must change accordingly. This is done by having different parameters for different data files. The following is an example of a file defining the calibration parameters for the S2 and S8-detectors, i.e. the time-of-flight detectors at the FRS.

```
LT_RANGE(”208 : 2 : 454: 1 : 3580 : 108570783”,”208 : 2 : 454: 1 : 3584 :
109558863”)
{
TIME_CALIB(SIGNAL_ID(SCI, 1, 1) , ( 219.859512, 0.048452),(0.1,0.1,0.0));
TIME_CALIB(SIGNAL_ID(SCI, 1, 2) , ( 224.243622, 0.047816),(0.1,0.1,0.0));
 TIME_CALIB(SIGNAL_ID(SCI, 2, 1) , ( 273.264404, 0.047842),(0.1,0.1,0.0));
TIME_CALIB(SIGNAL_ID(SCI, 2, 2) , ( 275.857910, 0.046547),(0.1,0.1,0.0));
}
LT_RANGE(”208 : 2 : 454 : 1 : 3585 : 109558864”,”208 : 2 : 454: 1 : 3589 :
110545854”)
{
TIME_CALIB(SIGNAL_ID(SCI, 1, 1) , ( 219.859512, 0.048463),(0.1,0.1,0.0));
TIME_CALIB(SIGNAL_ID(SCI, 1, 2) , ( 224.243622, 0.047828),(0.1,0.1,0.0));
 TIME_CALIB(SIGNAL_ID(SCI, 2, 1) , ( 273.264404, 0.047838),(0.1,0.1,0.0));
 TIME_CALIB(SIGNAL_ID(SCI, 2, 2) , ( 275.857910, 0.046537),(0.1,0.1,0.0));
 }
```

The numbers marked in red represent the run number, in green the file numbers and in blue the event numbers are given.

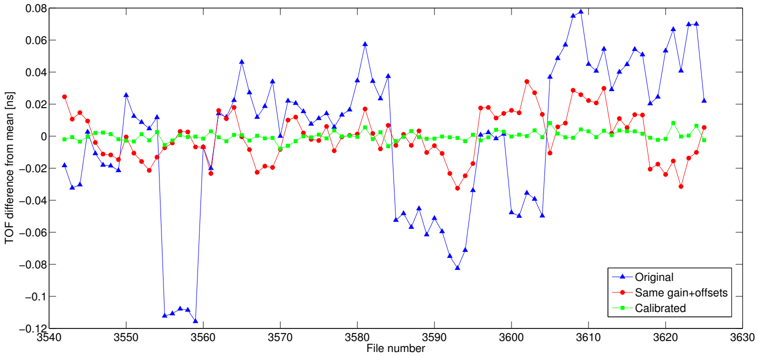

Figure 3.4: The difference of the incoming time-of-flight for one isotope relative to the mean of the entire run for the different files in one run. Blue triangles indicate the original calibration values, red dots the same calibration parameters for all files, and green squares when using identical gain but corrected offsets.

These numbers define for which events the following calibration parameters are valid. In this example the first calibration parameters are valid from run 454, file 3580, event 108570783 to run 454, file 3584 event 109558863. After that a new range is specified where slightly different calibration parameters are used. The calibration parameters themselves are specified by first specifying the type of calibration, in this case TIME_CALIB. Then the channel that is to be calibrated is given. The S8-detector is called SCI2 in the calibration, and since this detector has two channels, both have to be calibrated. Finally the calibration parameters are given as offset and gain values.

To check the calibration, the difference in the time-of-flight for a specific ion can be compared between different files. In Fig. 3.4 a comparison of the incoming time-of-flight for all files in one run is presented. Blue triangles indicate the difference in time from the mean of the run using the original calibration. These differences may not seem very large when the mean time-of-flight is around 250 ns, but they do affect the tracking. The main reason for these fluctuations is the difference in gain between the files. The first step is to use the same calibration parameters for all the files in the run, i.e. the same gain and offset. The result after this step is shown with red dots in Fig. 3.4. This clearly decreased the differences between the files. To further decrease the differences the offsets are changed according to the differences to the mean for each file. The result after this operation is indicated by green squares in Fig. 3.4. The improvement from the original calibration (blue triangles) is clear and the incoming velocity in the tracker is more stable for all files.

3.2.3 Detectors behind ALADIN

The first step in calibrating the detector positions behind ALADIN is to decide which incoming ion to use for the calibration, i.e. what charge and mass should it have. This is done utilising an identification plot (ID-plot) where the charge is plotted versus the mass over charge. Each ion can then be identified in terms of A and Z (Fig. 3.5). By applying a gate that the incoming ion has to be within a certain mass and charge according to this plot, the selection of the incoming ion is done. To further enforce that the selected ion is used, the energy loss in the SSTs can be exploited in the same way as the energy loss in the TFW was used earlier in Fig. 3.1. The selection is done by setting conditions on the parameters in a C++ file used by the tracker. The tracker uses only events, which fulfil all the conditions in this file. Conditions can be set on all parameters measured in the setup, both on incoming and outgoing fragments. For calibration it is the unreacted beam which is used, i.e. the incoming and outgoing ions have identical charge and mass. Hence an empty target run is best suited for calibration because this minimises the reaction probability. The incoming and outgoing charge can be selected with the SSTs and TFW as explained earlier. The outgoing mass cannot be selected, but since the reaction probability is minimised the vast majority of all ions do not react. This means that when looking at the mass of the tracked ions, given by the tracker, there is a large peak corresponding to unreacted ions, and possibly several small peaks corresponding to events where

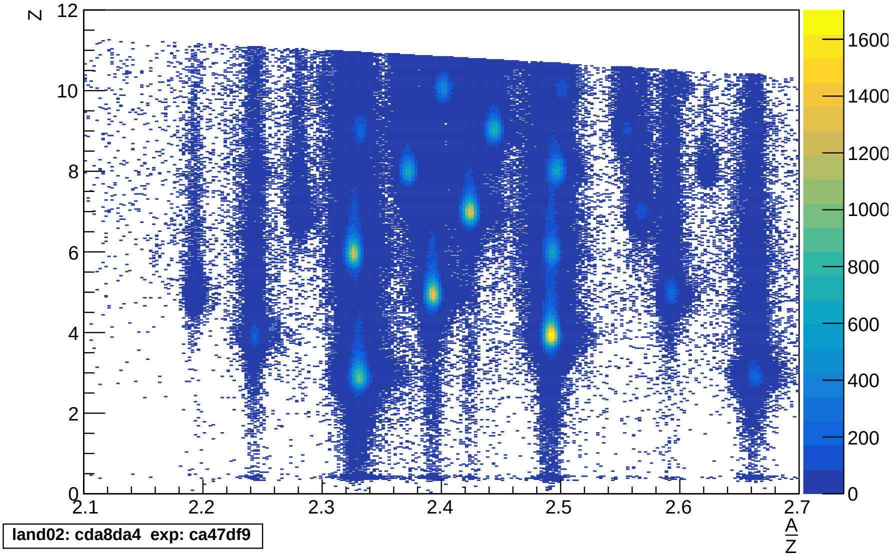

Figure 3.5: An ID-plot of the incoming ions. Each ion can be uniquely identified by its charge and mass over charge ratio.

reactions have occurred. After the right conditions have been set in the configuration file, the calibration can be performed using an automatic script. The script takes four arguments, the root-file which contains the data, the configuration file for the tracker, the charge of the ion to track which is selected in the C++ file and the mass of the ion, i.e. the number of nucleons.

The calibration script starts by running the tracker in forward mode, while the option to ignore the time-of-flight is chosen. The results that are interesting in this first part of the calibration are the residuals in the GFI and TFW, and the time offset. Due to the limited resolutions in the detectors, given that the ions may be scattered along their way, these residuals are never exactly zero but follow a Gaussian distribution. The residuals are retrieved by making fits to these distributions and taking the mean value. An example of how a plot of a

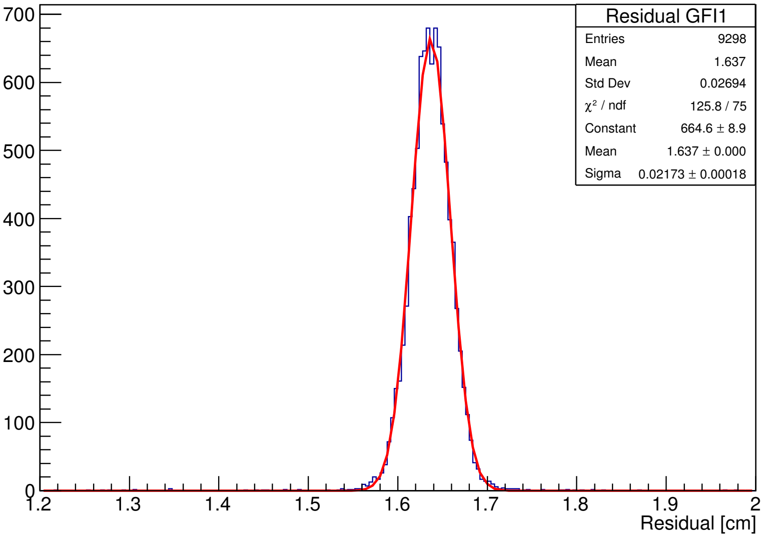

Figure 3.6: An example of the residual for the GFI1 in x-direction after tracking. The data are presented in blue and the Gaussian fit is given by the red line. In the status box the mean value of the fit can be seen at 1.637 cm.

residual looks is shown in Fig. 3.6. The detectors are moved according to their residuals by setting offsets to their positions in the configuration file. In the example given in Fig. 3.6, the detector would be moved 1.637 cm to set the mean value to zero. The same procedure is used for the time-of-flight. Since this parameter was not used in the tracking, because the tracking was performed with the option ignore time-of-flight, there is also a residual for the time-of-flight, which represents the difference between the measured time-of-flight and the calculated time-of-flight in the tracker. This residual is used to provide a time offset for the configuration file. When all the offsets are adjusted, the calibration script runs the tracker again with the new detector positions. After this tracking, all the residuals should be very close to zero.

What is interesting in this step is the mass of the tracked fragment. The measured masses follow also a Gaussian distribution and hence the value to use is the mean of the Gaussian fit. An example of the mass plot is shown in Fig. 3.7, along with a Gaussian fit.

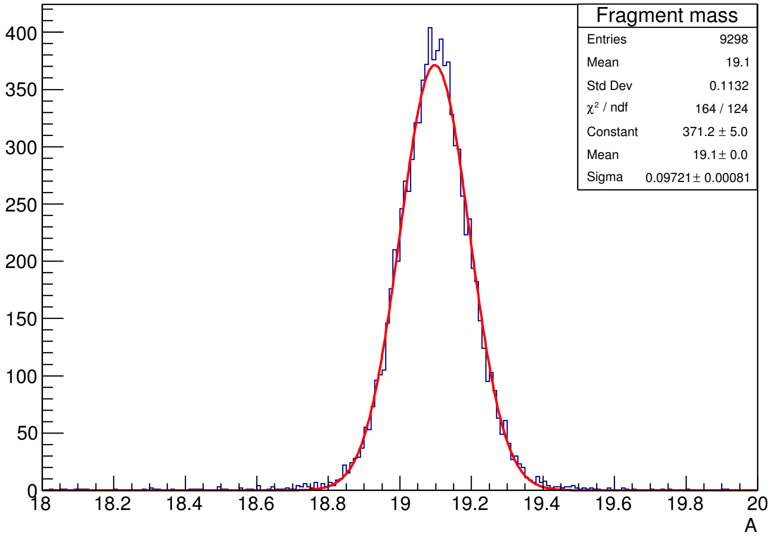

Figure 3.7: The mass of the tracked fragment given by the tracker. The fit, in red, is used to obtain the mean value of the distribution, which is in this case 19.1 mass units.

Since it is known what fragment is being tracked, its mass is also known. In the example given in Fig. 3.7, the tracked fragment is ^{19}O. The conclusion from the spectrum and fit is that the tracker in this case gives results which are 0.1 mass units too high. To fix this, the calibration script runs the tracker again, but now it uses a special mode called *have/want*. To run in this mode the tracker still needs the configuration file with the detector positions and if the tracking should be done in forward or in backward mode. What is special now is that two more options are given, namely the *have* and the *want* options.

In the *have* option, the present state of the tracker is given, i.e. the mass of the fragment and the incoming beta. In the *want* option, the values that are expected are entered while the *have* option specifies the present result from the tracker. Using the same example as before with ^{19}O, in the *have* option the mass 19.1 would be given and in the *want* option the mass would be set to 19.0. The tracker performs two calculations, one with the values given in *have* and one with the values from *want*. It then compares the hit positions in the GFIs and TFW and calculates how these should be moved to obtain the results specified in the *want* option. The calibration script takes these values and calculates new offsets to write to the configuration file. The last thing the calibration script does is to run the tracker again with the new detector positions and verifies that the mass from the tracker now agrees with the expected mass.

When the calibration is complete, the tracker can be used to track any ion. The only thing that should be changed after the calibration is the selection which ions to track in the C++ file, and possibly the magnet current in the configuration file, if the magnetic field has been changed between runs. If that is the case it is not certain that the magnet current set in the configuration file should be exactly the same as was set in the experiment. This has several reasons as discussed in Sec. 2.2.3. To find out what magnet current should be used, the tracker can be run for a single ion and check where the mass peak appears. If the peak is not where it is expected, the current can be changed to compensate for this, at least within some tens of amperes.

3.3 Outlook

The problem with the tracker calibration right now is that it divides the calibration into two parts, one in front of and one behind ALADIN. It would be better to calibrate the entire system at once. This can be done by including the GFIs and TFW in the alignment with Millepede and calculating the necessary residuals and derivatives in the tracker. The work of implementing this has already started. Thanks to R. Plag the tracker now calculates the derivatives and residuals needed by Millepede, and thanks to H. Törnqvist these values can be read and delivered to Millepede. The author has produced a script that makes use of these variables, but this work is still in progress. One of the main problems is to decide how to fix the detector positions in space. This was a problem also for the present alignment of the SSTs, as mentioned in Sec. 3.2.1, which was solved by fixing two detector positions. This solution would of course be possible also when extending the alignment to include the GFIs and TFW. The question is if this is the best solution or if there are other, better, methods. One possible solution is to perform the calibration several times with different detectors fixed and then try to combine the results.

What also potentially could improve the calibration is to take the z positions of the detectors into account. At the moment, these positions are based on photogrammetry measurements[7] and are fixed throughout the entire calibration procedure. Tests with z positions determined by Millepede have been done. Unfortunately they have not been successful so far. It could also be argued that rotations of the detectors around the x and y axis should be included. This can easily be discarded by trigonometric calculations though. Since the detectors are aligned as good as possible from the beginning, the angles will be very small, probably no more than $\approx 1^\circ$. Assuming that this is a rotation around the y-axis the hit positions in the detector are slightly shifted in the x and z-direction. The SSTs are about 7 cm wide, so the maximum x-position a detector can measure is 3.5 cm. Hence the maximum shift is $3.5 \text{ cm} \cdot (1 - \cos(1^\circ)) = 5.3\ \mu\text{m}$ in x direction and $3.5 \text{ cm} \cdot \sin(1^\circ) = 610\ \mu\text{m}$ in z direction. The change in the x-direction is negligible because it is smaller than the detector resolution. The shift in the z-direction is larger but the effect of it is still small. That is because the incoming ions are travelling almost parallel to the z-axis. Hence the position change in the x direction is very small, even if the detector hit is located 600 μm upstream than before. With the same arguments also a rotation around the x-axis be neglected.

---

[7] So are the x and y positions, but as shown in this chapter, they can be improved.

Chapter 4

Gamma multiplicities

When all nucleons in a nucleus are placed in the lowest possible single-particle orbitals, the nucleus is in its ground state. Any change in the configuration results in an excited nucleus that has different properties compared to the ground state. The total energy of the nucleus increases and the angular momentum might change. When an excited nucleus decays, either to a lower excited state, to its ground state or to another nuclide, the excess energy has to be conserved. This is fulfilled by emitting either nucleons, gamma rays or conversion electrons with the corresponding excitation energy difference. When a gamma is emitted the change in angular momentum between the initial and final state of the nucleus has to be at least $1\hbar$. If the difference in angular momentum is larger, the decay via gamma emission is still possible but becomes less probable with increasing angular momentum difference.

The gamma rays emitted from a decaying nucleus can give information about the structure of the nucleus. They can reveal information on the energy of a state, its parity, spin, angular momentum, lifetime, or the underlying nuclear structure to name a few. For a given angular momentum, there is a minimum excitation energy for a nucleus. This can be seen by plotting the excitation energy against the angular momentum and this limit is called the yrast line (see e.g. Ref. [28]) given by the collective rotational energy of the nucleus. The angular momentum of a nucleus is linearly proportional to the gamma multiplicity as shown in Ref. [29–31]. By measuring the gamma energy and multiplicity the relation between the excitation energy and the angular momentum can be studied.

Because of the linear relation with the angular momentum, the gamma multiplicity is often measured to study excited states with large angular momenta. These states can be populated in several different nuclear reactions. One common method is to use fusion-evaporation, but it is also possible to use incomplete fusion, deep inelastic scattering or fragmentation reactions [32]. The fragmentation method has the advantage of producing a wide range of isotopes [33] in contrast to the other methods where a single isotope is studied at a time. The problem is that the background in the gamma measurements becomes large [34, 35].

In this experiment cocktail beams with both proton and neutron rich nuclei, mostly unstable, ranging from Li to Ne were produced. This provides a good opportunity to compare the population and decay of excited states from different reaction channels. By identifying both the incoming and outgoing ion the reaction channel can be found. The reaction target is surrounded by a 4π-gamma detector, described in Sec. 2.2.2, with high granularity, which is able to measure the energy and multiplicity of the gammas emitted in a reaction in the target.

4.1 Reaction identification

To decide what reaction has occurred both the incoming and outgoing ions have to be identified. By comparing the mass and charge of the incoming and outgoing ions it is possible to decide if any reactions took place. As described in Sec. 3.2.3 the incoming ion can be identified by plotting the charge against the mass over charge ratio. To identify the outgoing ion the tracker is needed. The charge of the ion is given by the energy loss in the SSTs and TFW which is described in Sec. 3.1. After the tracker has been calibrated following the steps in Sec. 3.2 it provides the mass of the outgoing ion. When the reaction channel has been identified the gamma multiplicity also has to be determined.

One problem when measuring the gamma multiplicity is that the gammas may Compton scatter between different crystals, which means that the same gamma can deposit energy in several different crystals. This is a problem both for the multiplicities and the total energy deposition. To handle this problem a so called *add-back* routine is used for the Crystal Ball. This routine takes all the crystals that have been hit and sorts them into an array, by decreasing deposited energy. Then the routine takes the first crystal in the array, i.e. the one with the highest energy, and checks if any of its neighbours are also in the array. If a neighbour is in the array the time differences between the signals of the crystals are compared. If they are within 30 ns, they are assumed to originate from the same gamma photon. The energies of the crystals are summed and considered as one cluster. Each cluster contributes with one gamma hit in the multiplicity count. The add-back routine then takes the next crystal which has not been added to a cluster already. The not yet used crystal creates its own cluster and checks in the same way as for the first crystal if any of its neighbouring crystals are in the array. This procedure continues until all the crystals that recorded an energy deposit, have been added to a cluster. For more information about the efficiency of different add-back routines in the Crystal Ball, see Ref. [36], and for further details on the used add-back routine, see Ref. [37]. Since the Crystal Ball also detects protons and neutrons, scattered at large angles, this has to be considered when counting the gamma multiplicity as well. Gammas usually deposit less energy in the crystals than protons and neutrons, hence a condition on the energy deposition in the crystals can be used to exclude the latter. In the analysis a lower threshold on the deposited energies has also been applied. This is to avoid noise signals, contributing to the gamma multiplicity. Throughout the entire analysis this threshold is set to 0.1 MeV in all crystals.

4.2 Gamma multiplicities without a target

The background contribution to the multiplicity, can be obtained with a so-called empty target run where the reaction target has been removed from the beam line. That way the ions can only interact with the detector material in the beam path, which also can cause nuclear reactions. The incoming beam consists of many different ions. Because the background might depend on the ion species, it is necessary to select only events in the data that correspond to incoming ions of interest. This is done by applying conditions on the charge and the mass over charge ratio of the incoming ion. For the analysis in this section, ^{17}N has been chosen as an example, primarily because it has high statistics. The selection is done by performing a two-dimensional Gaussian fit to the data in the area, corresponding to ^{17}N. All events which are within 3 σ from the mean value of the fit are accepted as ^{17}N, while events outside this area are discarded. This selection is indicated in Fig. 4.1 by the red ellipse and has been used in all figures subsequent where the data for incoming ^{17}N has been plotted. In Fig. 4.2 the selection is used to show the number of crystals that fired in each event with incoming ^{17}N, and for comparison also offspill data are plotted. It is clear that most events are not associated with any or just a few crystals firing. However, there are also events where as many as 100 crystals fired in one event for both onspill and offspill data. What causes these high multiplicities? A good starting point is to check the energy signals of the crystals involved. In Fig. 4.3 the total event energy is plotted against the number of crystals, which has recorded a hit. In those plots it can be seen that the energy increases with the number of firing crystals, which is expected. What is not expected though, is the high energy deposits in the offspill data. The step structure for lower multiplicities is caused by overflows in the energy readouts from the crystals. The maximum readout energy for one crystal varies a lot, from about 5 MeV up to 40 MeV for some crystals. If an overflow is recorded the only energy information available is that the deposited energy exceeds the maximum readout energy. In this case 50 MeV has been added to the total energy if an overflow has been recorded. This limits the

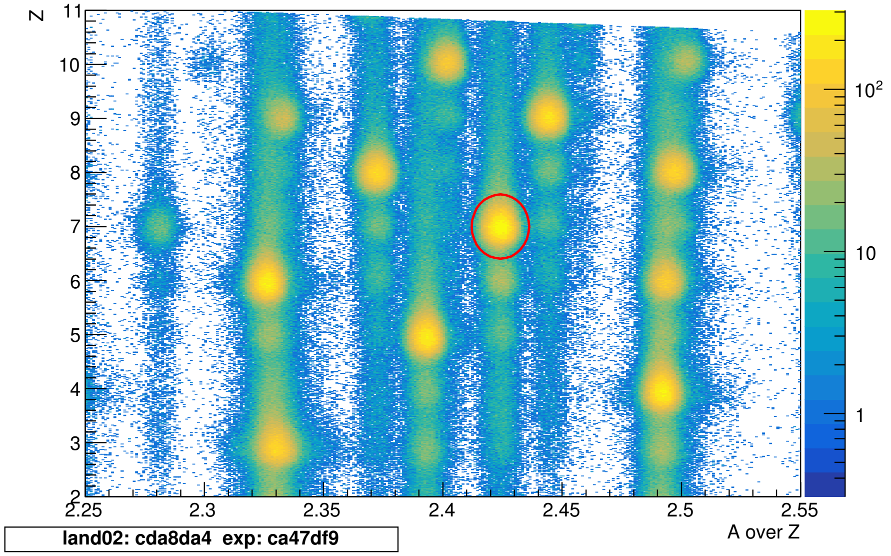

Figure 4.1: The selection of ^{17}N is indicated in the incoming ID-plot by the red ellipse.

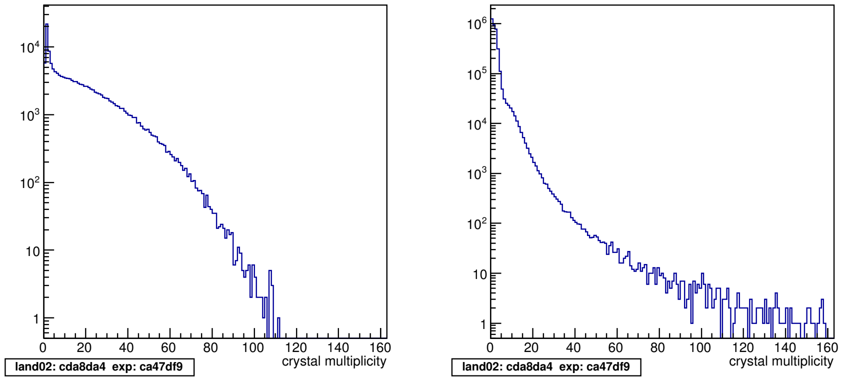

Figure 4.2: Crystal multiplicity in Crystal Ball with incoming ^{17}N to the left and with offspill data to the right.

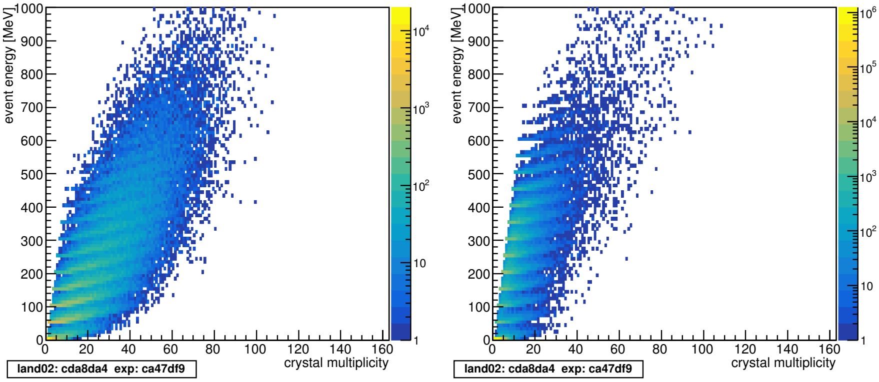

Figure 4.3: The total event energy summed over all crystals plotted versus the number of crystals that fired. The left figure shows the events for incoming ^{17}N, while on the right offspill data are plotted.

maximum energy in the plots to 50 MeV times the crystal multiplicity and this causes the step-like structure in the plots.

Since the energy deposition in the crystals cannot explain the the high multiplicities, it is necessary to investigate also the time measurements. All crystals record the time when they are hit relative to a common master start signal. In Fig. 4.4 the energy is plotted versus the time for all crystals. In this case the overflow signals are ignored. Here some structures can be observed, especially for the offspill data. There is a clear time interval where a majority of all hits happen, around −180 ns, both in onspill and offspill data. In the offspill data there are also many events that occur between −350 and −200 ns relative to the start, which feature structures in this time window. These structures become much more pronounced by looking at data from only one crystal, see Fig. 4.5, which displays data from crystal number 52, only. In the offspill data there are basically four different patterns, the previously noticed band at around −180 ns, another band at −300 ns and two bands with an exponential shape from −350 ns to −250 ns. In the onspill data there is also a band with an exponential shape at

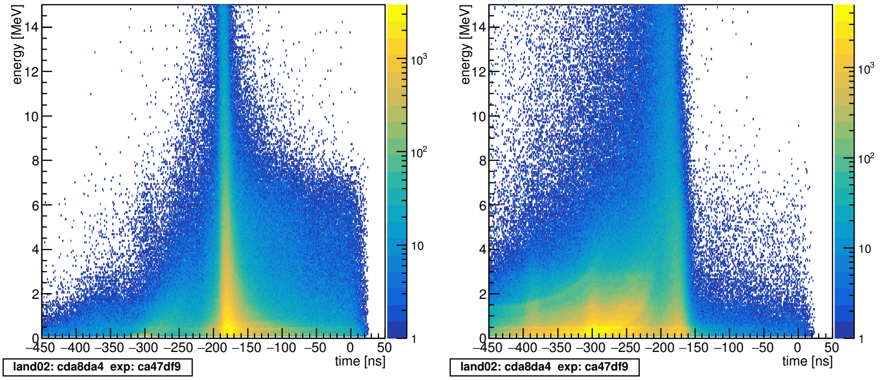

Figure 4.4: The energy versus the time for all crystals. Incoming ^{17}N nuclei were selected on the left. Offspill data are displayed in the right-hand figure.

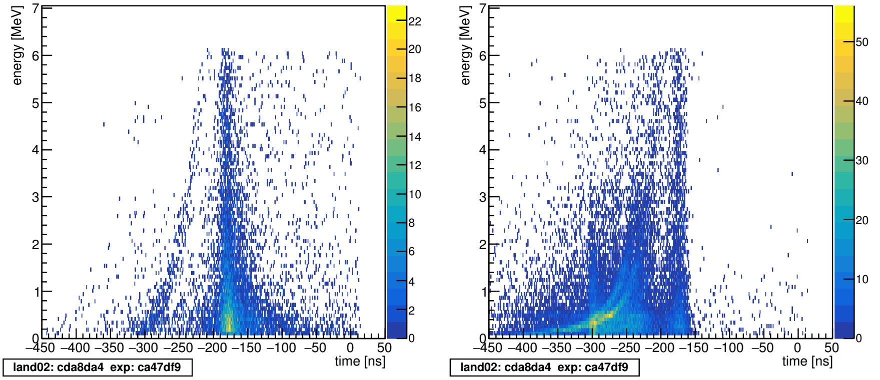

Figure 4.5: The energy versus time for crystal number 52. Incoming ^{17}N nuclei is shown in the left-hand figure, while offspill data are given to the right.

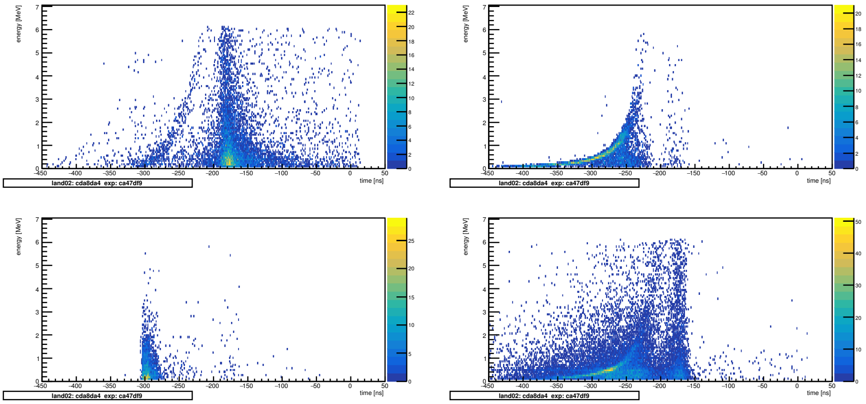

Figure 4.6: Energy versus time spectra for crystal number 52 for different trigger patterns. The top left figure represents data from Tpat 4, the top right figure from Tpat 9, the bottom left from Tpat 12 and the bottom right from Tpat 15.

the same time interval, even though it is not as pronounced as in the offspill data. The different structures can be related to different trigger patterns in the setup.

The Crystal Ball has four different trigger patterns, one for onspill and three for offspill data. In Fig. 4.6 the energy versus time for crystal number 52 is plotted again, but this time divided into the different trigger patterns involving the Crystal Ball. The top left figure is the onspill trigger while the other three are the different offspill triggers. The conditions for the different trigger patterns are explained in Tab. 2.2. The reason to have the different offspill triggers is that they are used for different types of calibration. Tpat numbers 9 and 15 are needed for calibrations with cosmic muons. Because muons are high-energy minimum-ionising particles, they traverse the entire Crystal Ball, hence at least two crystals are expected to fire. The third offspill trigger is used for calibration with a γ-source, which usually is placed in the centre of the Crystal Ball.

It is clear from the plots in Fig. 4.6 that the different structures in

Fig. 4.5 can be related to the different trigger patterns. For Tpat 4 there is hardly any difference compared to the plot with all onspill triggers, though. This means that this trigger is active in almost all events with an incoming ^{17}N ion. The question is if the structures in the plots can be used to discriminate the high multiplicity events shown in Fig. 4.2. One hypothesis was that the "real" hits were in the tail and that the others did not have any physical meaning originated from a background. When discriminating events in this way it looked promising at first, the high multiplicity events disappeared and the expected lower multiplicity events remained after a background subtraction. When this approach was applied also to runs with other ions, and with a reaction target inserted, it turned out that the hypothesis was wrong, though. Plotting the gamma multiplicity after background subtraction for other ions the number of events with multiplicity one or two became negative, while higher multiplicities up towards ten were positive. Since it is not reasonable to have a negative number of events, and especially not for multiplicities, which are expected to be the most common, this hypothesis was discarded. Instead another approach was used to find out where the "real" physics events are situated in the plot. This was done by using data from a reaction where an excited state with a known excitation energy was populated.

4.3 Gamma multiplicities with a target

The purpose of the target is to cause nuclear reactions with the incoming ions. At relativistic energies and impact parameters smaller than the radii of projectile and target, one or more nucleons are likely to be removed from the nucleus, creating a new isotope, typically in an excited state. To find out where the "real" events in the energy versus time plot ends up, the excited state in ^{10}C is used. It has an excitation energy of 3.355 MeV [38] and decays to the ground state by emitting one gamma photon. This state can be reached by knocking out one neutron from ^{11}C. By using the identification plot, selecting incoming ^{11}C, and using the tracker to match this with outgoing ^{10}C, this state

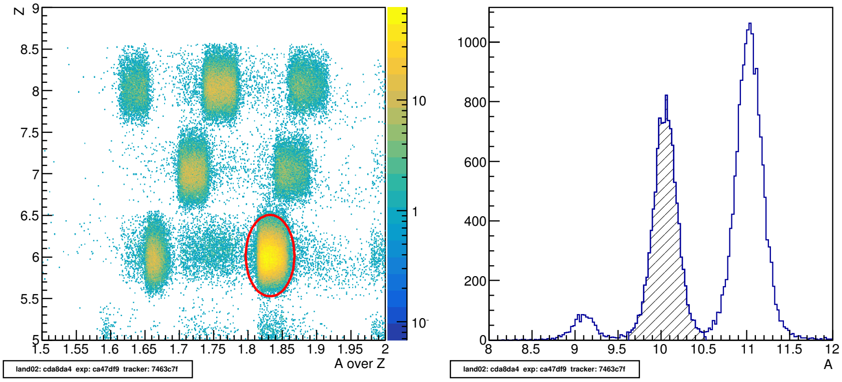

Figure 4.7: The selection of the incoming ^{11}C is indicated with the red ellipse to the left and the outgoing ^{10}C selection is indicated by the dashed area in the plot to the right.

can be found by looking at the energy deposited in Crystal Ball.

The selection of the incoming ^{11}C, done in the same way as for ^{17}N in the empty target case, is shown in Fig. 4.7. In the same figure the selection of the outgoing ^{10}C is also presented. Since the charge of the outgoing fragments is provided to the tracker as described in Sec. 3.1, only the mass needs to be selected in combination with a condition on the charge to be 6. In Fig. 4.7 the tracked mass is plotted for all ions with charge 6 while the incoming ions were identified as ^{11}C. The dashed area marks the selection of ^{10}C and contains all events within three sigma from the mean of a Gaussian fit to the mass peak.

The energy and time in the Crystal Ball are shown in Fig. 4.8 together with a projection of the energy. To obtain the correct gamma energy it is not sufficient to do the add-back of the crystals but it is also necessary to compensate for the Doppler effect, which is is discussed in Sec. 2.2.2. The projection plot is made by projecting all events in the time interval -205 to -167.5 ns onto the y-axis in the plot resulting in a one dimensional energy plot. In this plot the peak at 3.2 MeV which originates from the excited state in ^{10}C* can be seen. Hence it is clear

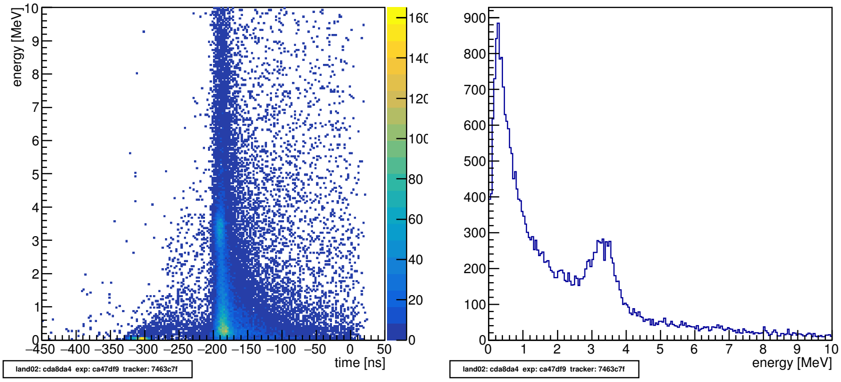

Figure 4.8: Plotted to the left is the Doppler corrected energy versus time for incoming ^{11}C and outgoing ^{10}C. To the right is a projection of the energy for times between -205 and -167.5 ns presented, where the excited state can be seen as a peak around 3.2 MeV.

that the gammas from the decay of ^{10}C* end up in this time interval and it can be assumed that this is where the relevant data is recorded. To verify this the gamma multiplicity can be checked. Since the 3.355 MeV state of ^{10}C decays to the ground state, only one gamma is expected, so the gamma multiplicity is expected to be one if only events with this energy are chosen. The multiplicity is shown in Fig. 4.9 where only events with gamma energies 3.23 ± 0.54 MeV and times between -205 and -167.5 ns are included. Since the Crystal Ball also is able to detect protons and to some extent neutrons, an additional condition is imposed on the energy in a hit to be less than 20 MeV to contribute to the multiplicity. This is expected to be sufficient to avoid excluding any gammas, but discriminates heavier particles. The expectation was that the gamma multiplicity would be close to one, but here the peak is at multiplicity two and there is a long tail up to multiplicity 20. This tail is problematic because it makes it impossible to draw any conclusions about the gamma multiplicity for this reaction. The same problem can be seen also in other reactions where the expected gamma multiplicity

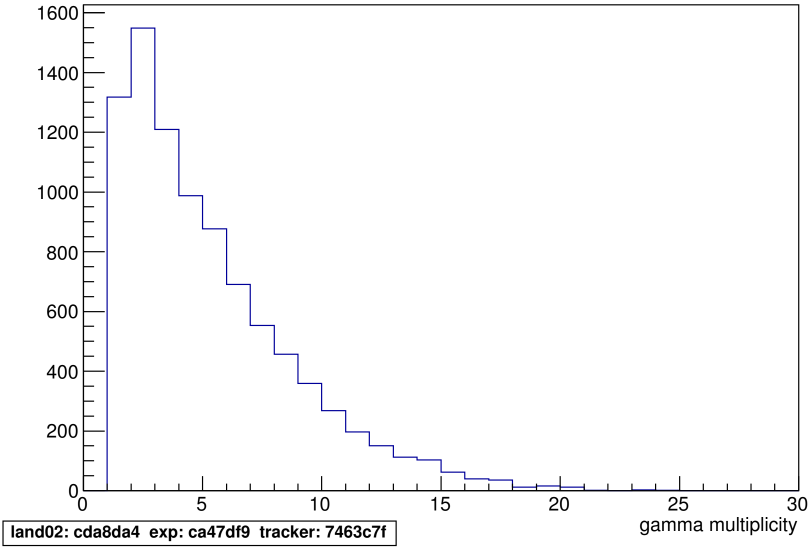

Figure 4.9: The gamma multiplicity in the Crystal Ball for events with gamma energy 3.23 ± 0.54 MeV and times between -205 and -167.5 ns

.

is known but there is a tail in the plot.

Right now there seems to be no way to suppress this tail. There are probably only two different explanations to this. One is that the Crystal Ball actually detects the correct multiplicity but there are more reactions involved, adding extra gammas. The second is that there are some problems with the Crystal Ball or its electronics, causing the high multiplicities. The most likely is that the Crystal Ball works well but there are additional reactions causing more gammas. The strongest argument for this is that the expected excitation energy can be seen in Fig. 4.8 meaning that the Crystal Ball measures correct energies.

A possible explanation to the high multiplicities could be that they are caused by gamma flashes, which have been reported as major problems in gamma-spectroscopy experiments at GSI [39, 40]. This effect creates lots of photons, but they do not carry much energy, typically less than 1 MeV. In Fig. 4.3 the total energy deposited in the Crystal Ball is shown for each event, and for higher multiplicities these are several 100 MeV. It can also be seen in Fig. 4.4 that the energy deposited in single crystals varies a lot and energies of several MeV are common. When comparing the gamma multiplicities between data taken with a lead target and data with a carbon target, no major differences can be observed. If the gamma flash would have any major impact on the multiplicity measurement it is expected to be stronger for the lead target than the carbon target. These observations cannot completely exclude the impact of gamma flashes on the multiplicity measurements, but based on the energies involved and the similarities in the gamma multiplicities with the different targets, gamma flashes alone cannot explain the origin of the high multiplicity events.

One possible problem with the Crystal Ball could be that some crystals trigger more often than others, causing the higher multiplicities. In Fig. 4.10 the crystal number is plotted versus the gamma multiplicity. There are obviously crystals that trigger more often than others, but this is also expected since those are the ones in the forward direction. Note that the multiplicity does not depend on the individual crystal number. The relative trigger rate of all crystals is the same for all multiplicities.

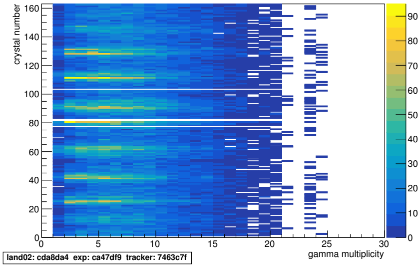

Figure 4.10: The crystal number plotted versus the gamma multiplicity in the Crystal Ball.

Another thing that also has to be excluded is activation inside the Crystal Ball. For example, if a detector frame is hit by the beam it can be activated and continuously emit gammas. This would of course affect the gamma multiplicity depending on how much material is activated. One way to verify that the frames of the SSTs are not hit is simply to examine the hit positions in those detectors. The beam is quite broad but still centred in all the detectors. This would imply that only very few ions hit the frame potentially activating the material. To further confirm this statement the crystal multiplicity in the Crystal Ball can be plotted for a cosmic run, i.e. data taken when no beam is present. The crystal multiplicity in a cosmic run is shown in Fig. 4.11 and is very similar to the multiplicity of the offspill data in Fig. 4.2. Since no beam is present in the cosmic run, the detector frames cannot be activated and cause high multiplicities. For offspill data the beam has been on just a second earlier, meaning that if something in the setup has been hit it is likely to still be activated. If the possible activation has any effect on the multiplicity measurements, a larger difference between the offspill and cosmic run measurements is expected. One last thing that

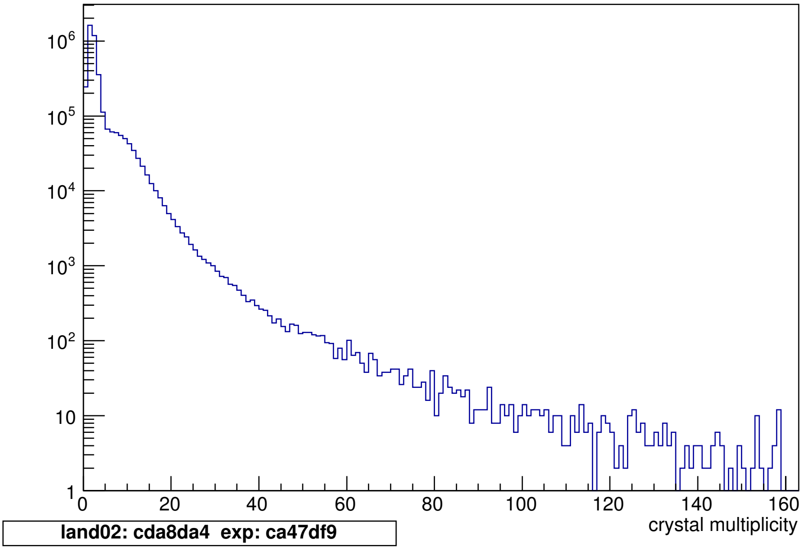

Figure 4.11: The number of crystals fired in the Crystal Ball during a background measurement. In this figure all events with a trigger pattern involving the Crystal Ball have been used.

can be interesting to investigate is whether the high multiplicities have been present also in earlier experiments or if it is something that is specific for this experiment. It turns out by looking at Fig. 4.12 where the crystal multiplicity is plotted for a cosmic run during experiment S327, which was performed in 2008, that this is not a new phenomenon. Both the multiplicity and energy versus time plots look similar to the experiment of this work. The high multiplicities seem to have been present also in earlier experiments.

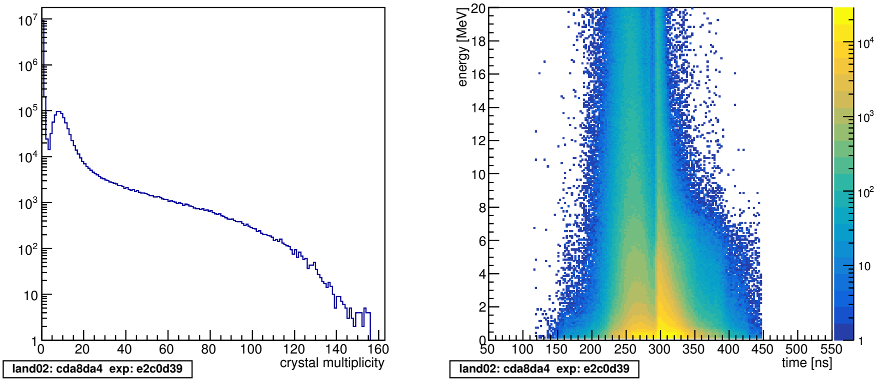

Figure 4.12: To the left is the crystal multiplicity in a cosmic run during experiment S327 and to the left is the energy plotted versus the time for the same run and experiment.

4.4 Summary

The goal of this work was to investigate the gamma multiplicity in different reaction channels from lithium up to neon. The gammas in the reactions are measured by the Crystal Ball, which encloses the target almost completely. Due to the relatively high granularity of the Crystal Ball it is possible to distinguish different gammas from each other which in turn makes it possible to count the number of gammas in an event. It turned out though, when starting to evaluate the data that there are a significant number of events with unreasonably high gamma multiplicities which can be seen in Fig. 4.2 and 4.11. The origin of the high multiplicities is still not completely clear. No correlation has been found between the high multiplicities and any other measured quantities such as deposited energy, which crystals fire or timing of the hits. The only correlation that has been found, is between the deposited energy and the recorded time in a crystal, which can be seen in Fig. 4.6. Depending on the trigger, the correlation looks different. For the onspill data there is only one trigger pattern that involves the Crystal Ball, Tpat 4. In the figure, two different structures can be seen, one where time is independent of the deposited energy around, -200 to -160 ns, and one where the time increase with higher energies starting around -300 ns. When the same plot is obtained for a specific reaction where an excited state in ^{10}C can be populated, the excited state can be seen slightly above 3 MeV, which is the expected excitation energy. It can also be seen that the corresponding energy is only found in the time interval between -200 and -160 ns. Since this is the same time interval where most of the statistics can be found, it is not possible to disentangle the events originating from an excited state from what would be considered background, without knowing the excitation energy. Even worse is, that even if a condition is set to only use events where a gamma with the right energy and time has been recorded, the gamma multiplicity in those events still can be very high. This is shown in Fig. 4.9 where a long tail can be seen up towards 20 gammas in one event. So the question remains, what causes the high multiplicities? At this moment no answer can be given to that question. The most plausible explanation at this point would be that there occurs a reaction producing a shower of gammas. That would of course not explain the high multiplicities in the offspill data but there it could instead be cosmic muons reacting with the concrete shielding the cave creating showers hitting all over the Crystal Ball. This theory can be confirmed by checking if other detectors of the setup, such as LAND, also see such showers in coincidence, but this has not been done yet. The conclusion about the gamma multiplicities is that extracting them from the data is not possible due to too much background with an origin that is still not understood.

Chapter 5

Summary

A new method for virtually aligning the tracking detectors in the LAND-setup has been presented in Ch. 3. It performs the alignment in two steps. First are the SSTs in front of ALADIN aligned using the measured tracks of the incoming nuclei in combination with the program Millepede II. After that, the detectors behind ALADIN are aligned based on the tracks given from the SSTs aligned in the first step. For this task the TRACKER is used, which is a program developed for tracking ions through ALADIN and in the end for extracting the masses of the reaction fragments based on their magnetic rigidity and energy-loss. Before the TRACKER can be used, though, the incoming time-of-flight has to be calibrated. This is because the magnetic rigidity of the fragments depends on the velocity and hence the tracking through ALADIN is sensitive to velocity fluctuations originating from the time-of-flight measurements. How the time-of-flight calibration is done is explained in Sec. 3.2.2. This new alignment method is applied by running three different scripts, which make it easier to use compared to previous methods. An improved method is also in development. It relies on the same technique as presented in this thesis, but instead of dividing the alignment into two parts, it takes the entire setup at once.

In Ch. 4 the possibilities of measuring the gamma multiplicities originating from a wide range of radioactive beams, including both proton- and neutron-rich nuclei from Li to F, were investigated. When analysing the data a massive background contribution for the gamma multiplicity measurements was found, resulting in events with gamma multiplicities of more than 20. The origin of this background has been systematically investigated, but is still unclear at this point. Excited states can be seen in the energy spectra, meaning that the detector measures correct energies. Possible background contributors are discussed, e.g. gamma flashes and activation of material in detector support structures. Correlations between energy depositions and timing measurements in the crystals have been found where different structures in the plots could be connected to different trigger patterns. These correlations could not be exploited to suppress background gammas, though. A hypothesis at this point is that the high multiplicities originate from violent nuclear reactions in the target or from showers created by cosmic muons in the concrete shielding of the roof of the experimental area.

Glossary

add-back	Routine used in Crystal Ball for summing energies of several crystals originating from the same initial gamma photon.
ALADIN	A Large Acceptance DIpole magNet, the magnet used in the LAND-setup to separate reaction products.
C++	A programming language in which the majority of all scripts used in the analysis in this thesis have been written.
CALIFA	CALorimeter for In Flight detection of gamma-rays and high energy charged pArticles, the new gamma detector under construction to replace the Crystal Ball.
DAQ	Data AcQuisition, the system used for handling and storing data from the detectors.
DHIT	Unpack level in LAND02.
ESR	Experimental Storage Ring.
FAIR	Facility for Antiproton and Ion Research, a new international facility located at the site of GSI.
FRS	FRagment Separator, used to separate and identify radioactive beams produced in reactions from stable beams at GSI.

GFI	Grosser FIber detector, a position sensitive fibre detector used in the LAND-setup to track reaction fragments.
GSI	Gesellschaft für SchwerIonenforschung, The research centre where the experiment was performed, located in Darmstadt, Germany.
have/want	Two options given to the TRACKER for calibration of the setup.
HIT	Unpack level in LAND02.
LAND	Large Area Neutron Detector, the neutron detector used in the experimental setup.
LAND02	The program package for unpacking data stored in lmd-files.
Millepede II	Program used to align detectors.
PMT	Photo Multiplier Tube, converts light into electrical signal via the photoelectric effect and photo-electron multiplication.
POS	POSition detector, used for time-of-flight measurements in the setup.
RAW	Unpack level in LAND02.
ROLU	Rechts-Oben-Links-Unten, veto detector for discriminating incoming ions to far from the beam centre.
S393	Identification number of the analysed experiment.
SCI2	SCIntilator 2, detector placed at the end of the FRS for time-of-flight measurements.
SIS18	SchwerIonen Synchrotron, the synchrotron used to accelerate ions to relativistic energies at GSI.

SST	Silicon Strip deTector, double-sided silicon strip detectors placed around the target for tracking and energy-loss measurements.
SYNC	Unpack level in LAND02.
TCAL	Unpack level in LAND02.
TFW	Time-Of-flight Wall, array of plastic scintillator detectors used for time-of-flight and energy loss measurements.
Tpat	Number defining the triggers involved in the event.
TRACK	Unpack level in LAND02.
the TRACKER	Program used to track reaction fragments through ALADIN to obtain mass of fragments and aligning detectors.
UNILAC	UNIversal Linear ACcelerator, first accelerator used before ions can be sent into the synchrotron.
XB	Crystal Ball, the 4π-gamma detector made of 159 NaI(Tl) crystals surrounding the target.

Bibliography

[1] O. Haxel, J. H. D. Jensen, and H. E. Suess, "On the "magic numbers" in nuclear structure," *Phys. Rev.*, vol. 75, pp. 1766–1766, Jun 1949.

[2] M. G. Mayer, "On closed shells in nuclei. ii," *Phys. Rev.*, vol. 75, pp. 1969–1970, Jun 1949.

[3] R. Casten, *Nuclear Structure from a Simple Perspective.* Oxford University Press, 2001.

[4] G. Hagen, T. Papenbrock, D. J. Dean, and M. Hjorth-Jensen, "*Ab initio* coupled-cluster approach to nuclear structure with modern nucleon-nucleon interactions," *Phys. Rev. C*, vol. 82, p. 034330, Sep 2010.

[5] Y. Utsuno, T. Otsuka, T. Mizusaki, and M. Honma, "Varying shell gap and deformation in $N \sim 20$ unstable nuclei studied by the Monte Carlo shell model," *Phys. Rev. C*, vol. 60, p. 054315, Oct 1999.

[6] M. Hjorth-Jensen, T. T. Kuo, and E. Osnes, "Realistic effective interactions for nuclear systems," *Physics Reports*, vol. 261, no. 3–4, pp. 125 – 270, 1995.

[7] W. Dickhoff and C. Barbieri, "Self-consistent Green's function method for nuclei and nuclear matter," *Progress in Particle and Nuclear Physics*, vol. 52, no. 2, pp. 377 – 496, 2004.

[8] "Riken Nishina Center for Accelerator-Based Science." `http://www.nishina.riken.jp/RIBF`, 2016.

[9] "GSI Helmholtzzentrum für Schwerionenforschung GmbH." `https://www.gsi.de/en/`, 2016.

[10] "Facility for Antiproton and Ion Research in Europe GmbH." `http://www.fair-center.eu`, 2016.

[11] The R^3B Collaboration, "Technical Report for the Design, Construction and Commissioning of The CALIFA Barrel: The R^3B CALorimeter for In Flight detection of γ-rays and high energy charged pArticles," tech. rep., FAIR, November 2011. `http://www.fair-center.eu/fileadmin/fair/publications_exp/CALIFA_BARREL_TDR_web.pdf`.

[12] The R^3B Collaboration, "The R^3B CALorimeter for In Flight detection of γ-rays and high energy charged pArticles – Technical Report for the Design, Construction and Commissioning of The CALIFA Endcap," tech. rep., FAIR, August 2015. `http://www.fair-center.eu/fileadmin/fair/experiments/NUSTAR/Pdf/TDRs/TDR_R3B_CALIFA_ENDCAP_public.pdf`.

[13] The R^3B Collaboration, "Technical Report for the Design, Construction and Commissioning of NeuLAND: The High-Resolution Neutron Time-of-Flight Spectrometer for R^3B," tech. rep., FAIR, November 2011. `http://www.fair-center.eu/fileadmin/fair/experiments/NUSTAR/Pdf/TDRs/NeuLAND-TDR-Web.pdf`.

[14] R. Palit, P. Adrich, T. Aumann, K. Boretzky, B. V. Carlson, D. Cortina, U. Datta Pramanik, T. W. Elze, H. Emling, H. Geissel, M. Hellström, K. L. Jones, J. V. Kratz, R. Kulessa, Y. Leifels, A. Leistenschneider, G. Münzenberg, C. Nociforo, P. Reiter, H. Simon, K. Sümmerer, and W. Walus, "Exclusive measurement of breakup reactions with the one-neutron halo nucleus ^{11}Be," *Phys. Rev. C*, vol. 68, p. 034318, Sep 2003.

[15] H. Geissel, P. Armbruster, K. Behr, A. Brünle, K. Burkard, M. Chen, H. Folger, B. Franczak, H. Keller, O. Klepper, B. Langenbeck, F. Nickel, E. Pfeng, M. Pfützner, E. Roeckl, K. Rykaczewski, I. Schall, D. Schardt, C. Scheidenberger, K.-H. Schmidt, A. Schröter, T. Schwab, K. Sümmerer, M. Weber, G. Münzenberg, T. Brohm, H.-G. Clerc, M. Fauerbach, J.-J. Gaimard, A. Grewe, E. Hanelt, B. Knödler, M. Steiner, B. Voss, J. Weckenmann, C. Ziegler, A. Magel, H. Wollnik, J. Dufour, Y. Fujita, D. Vieira, and B. Sherrill, "The GSI projectile fragment separator (FRS): a versatile magnetic system for relativistic heavy ions," *Nuclear Instruments and Methods in Physics Research Section B: Beam Interactions with Materials and Atoms*, vol. 70, no. 1, pp. 286 – 297, 1992.

[16] G. Münzenberg, "The separation techniques for secondary beams," *Nuclear Instruments and Methods in Physics Research Section B: Beam Interactions with Materials and Atoms*, vol. 70, no. 1, pp. 265 – 275, 1992.

[17] R. Plag, "Land02, the unofficial guide to the unofficial version of land02." `web-docs.gsi.de/~rplag/land02`.

[18] V. Metag *et al.*, "The Darmstadt-Heidelberg-Crystal-Ball," in *Proc. Geiger Memorial Meeting*, October 1982.

[19] T. Blaich *et al.*, "A large area detector for high-energy neutrons," *Nuclear Instruments and Methods in Physics Research A*, vol. 314, pp. 136–154, 1992.

[20] J. Cub, G. Stengle, A. Grünschloss, K. Boretzky, *et al.*, "A large-area scintillating fibre detector for relativistic heavy ions," *Nuclear Instruments and Methods in Physics Research A*, vol. 402, pp. 67–74, 1998.

[21] R. Brun and F. Rademakers, "ROOT — an object oriented data analysis framework," *Nuclear Instruments and Methods in Physics Research Section A: Accelerators, Spectrometers, Detectors and*

Associated Equipment, vol. 389, no. 1–2, pp. 81 – 86, 1997. New Computing Techniques in Physics Research V.

[22] H. Johansson, *The DAQ always runs.* Licentiate thesis, Chalmers University of Technology, 2006.

[23] L. Råde and B. Westergren, *Mathematics Handbook.* Studentlitteratur, fifth ed., 2004.

[24] R. Plag, "Some documentation on ralf's tracker." `http://ralfplag.de/tracker`, 2016.

[25] R. Plag. Private communication, April 2016.

[26] R. Plag. Private communication, January 2015.

[27] V. Blobel, "Software alignment for tracking detectors," *Nuclear Instruments and Methods in Physics Research Section A: Accelerators, Spectrometers, Detectors and Associated Equipment*, vol. 566, no. 1, pp. 5 – 13, 2006.

[28] A. Bohr, "Rotational motion in nuclei," *Rev. Mod. Phys.*, vol. 48, pp. 365–374, Jul 1976.

[29] S. Gil, R. Vandenbosch, A. J. Lazzarini, D.-K. Lock, and A. Ray, "Spin distribution of the compound nucleus in heavy ion reactions at near-barrier energies," *Phys. Rev. C*, vol. 31, pp. 1752–1762, May 1985.

[30] A. B. Balantekin and P. E. Reimer, "Determination of an effective radius from the gamma-ray multiplicities in fusion reactions," *Phys. Rev. C*, vol. 33, pp. 379–381, Jan 1986.

[31] G. Henning, T. L. Khoo, A. Lopez-Martens, D. Seweryniak, M. Alcorta, M. Asai, B. B. Back, P. F. Bertone, D. Boilley, M. P. Carpenter, C. J. Chiara, P. Chowdhury, B. Gall, P. T. Greenlees, G. Gürdal, K. Hauschild, A. Heinz, C. R. Hoffman, R. V. F. Janssens, A. V. Karpov, B. P. Kay, F. G. Kondev, S. Lakshmi,

T. Lauritsen, C. J. Lister, E. A. McCutchan, C. Nair, J. Piot, D. Potterveld, P. Reiter, A. M. Rogers, N. Rowley, and S. Zhu, “Fission barrier of superheavy nuclei and persistence of shell effects at high spin: Cases of ^{254}No and ^{220}Th,” *Phys. Rev. Lett.*, vol. 113, p. 262505, Dec 2014.

[32] P. Walker and G. Dracoulis, “Energy traps in atomic nuclei,” *Nature*, vol. 399, pp. 35–40, May 1999.

[33] R. Grzywacz, R. Anne, G. Auger, D. Bazin, C. Borcea, V. Borrel, J. Corre, T. Dörfler, A. Fomichov, M. Gaelens, D. Guillemaud-Mueller, R. Hue, M. Huyse, Z. Janas, H. Keller, M. Lewitowicz, S. Lukyanov, A. Mueller, Y. Penionzhkevich, M. Pfützner, F. Pougheon, K. Rykaczewski, M. Saint-Laurent, K. Schmidt, W.-D. Schmidt-Ott, O. Sorlin, J. Szerypo, O. Tarasov, J. Wauters, and J. Żylicz, “Identification of μs-isomers produced in the fragmentation of a ^{112}Sn beam,” *Physics Letters B*, vol. 355, no. 3–4, pp. 439 – 446, 1995.

[34] S. Wan, J. Gerl, J. Cub, J. Holeczek, P. Reiter, D. Schwalm, T. Aumann, K. Boretzky, W. Dostal, B. Eberlein, H. Emling, C. Ender, T. Elze, H. Geissel, A. Grünschloß, R. Holzmann, N. Iwasa, M. Kaspar, A. Kleinböhl, O. Koschorrek, Y. Leifels, A. Leistenschneider, I. Peter, H. Schaffner, C. Scheidenberger, R. Schubart, R. Schubert, H. Simon, G. Stengel, A. Surowiec, and H. Wollersheim, “In-beam γ-spectroscopy with relativistic radioactive ion beams,” *The European Physical Journal A - Hadrons and Nuclei*, vol. 6, no. 2, pp. 167–174, 1999.

[35] S. Wan, P. Reiter, J. Cub, H. Emling, J. Gerl, R. Schubart, and D. Schwalm, “γ-spectroscopy of light neutron-rich nuclei after secondary reactions at relativistic energies,” *Zeitschrift für Physik A Hadrons and Nuclei*, vol. 358, no. 2, pp. 213–215, 1997.

[36] S. Lindberg, “Optimised use of detector systems for relativistic radioactive beams,” Master’s thesis, Chalmers University of Technology, 2013.

[37] R. Thies, *Across the Dripline and Back: Examining* ^{16}B. Licentiate thesis, Chalmers University of Technology, 2014.

[38] D. R. Tilley, J. H. Kelley, J. L. Godwin, D. J. Millener, J. E. Purcell, C. G. Sheu, and H. R. Weller, “Energy levels of light nuclei A=8, 9, 10,” *Nuclear Physics A*, vol. 745, no. 3–4, pp. 155–362, 2004.

[39] P. Detistov, D. L. Balabanski, and Z. Podolyák, “Simulation of the electromagnetic background radiation for the RISING experimental set-up,” *Acta Physica Polonica B*, vol. 38, no. 4, p. 1287, 2007.

[40] S. Pietri *et al.*, “First results from the stopped beam isomer RISING campaign at GSI,” *Acta Physica Polonica B*, vol. 38, no. 4, p. 1255, 2007.